



Calhoun: The NPS Institutional Archive
DSpace Repository

NPS Scholarship

Theses

2002-06

Variability of refractivity in the surface layer

Mabey, Deborah L.

Monterey, California. Naval Postgraduate School

<https://hdl.handle.net/10945/5877>

This publication is a work of the U.S. Government as defined in Title 17, United States Code, Section 101. Copyright protection is not available for this work in the United States.

Downloaded from NPS Archive: Calhoun



Calhoun is the Naval Postgraduate School's public access digital repository for research materials and institutional publications created by the NPS community. Calhoun is named for Professor of Mathematics Guy K. Calhoun, NPS's first appointed -- and published -- scholarly author.

Dudley Knox Library / Naval Postgraduate School
411 Dyer Road / 1 University Circle
Monterey, California USA 93943

<http://www.nps.edu/library>

NAVAL POSTGRADUATE SCHOOL Monterey, California



THESIS

**VARIABILITY OF REFRACTIVITY IN THE SURFACE
LAYER**

by

Deborah L. Mabey

June 2002

Thesis Advisor:

K. Davidson

Co-Advisor:

P. Guest

Approved for public release; distribution is unlimited.

THIS PAGE INTENTIONALLY LEFT BLANK

REPORT DOCUMENTATION PAGE			Form Approved OMB No. 0704-0188	
Public reporting burden for this collection of information is estimated to average 1 hour per response, including the time for reviewing instruction, searching existing data sources, gathering and maintaining the data needed, and completing and reviewing the collection of information. Send comments regarding this burden estimate or any other aspect of this collection of information, including suggestions for reducing this burden, to Washington headquarters Services, Directorate for Information Operations and Reports, 1215 Jefferson Davis Highway, Suite 1204, Arlington, VA 22202-4302, and to the Office of Management and Budget, Paperwork Reduction Project (0704-0188) Washington DC 20503.				
1. AGENCY USE ONLY (Leave blank)		2. REPORT DATE June 2002	3. REPORT TYPE AND DATES COVERED Master's Thesis	
4. TITLE AND SUBTITLE: Variability of Refractivity in the Surface Layer			5. FUNDING NUMBERS	
6. AUTHOR(S) LT Deborah L. Mabey				
7. PERFORMING ORGANIZATION NAME(S) AND ADDRESS(ES) Naval Postgraduate School Monterey, CA 93943-5000			8. PERFORMING ORGANIZATION REPORT NUMBER	
9. SPONSORING /MONITORING AGENCY NAME(S) AND ADDRESS(ES) N/A			10. SPONSORING/MONITORING AGENCY REPORT NUMBER	
11. SUPPLEMENTARY NOTES The views expressed in this thesis are those of the author and do not reflect the official policy or position of the Department of Defense or the U.S. Government.				
12a. DISTRIBUTION / AVAILABILITY STATEMENT Approved for public release; distribution is unlimited.			12b. DISTRIBUTION CODE	
13. ABSTRACT (maximum 200 words) The author and members of the Boundary Layer Studies Group collected atmospheric surface layer profile properties affecting RF propagation during the Roughness and Evaporation Duct experiment off the windward coast of Oahu. We measured temperature, humidity and pressure profiles from the surface and up to 100 m by multi-level buoy-mounted sensors and a rawinsonde attached to a kite flown from a small vessel. We obtained the profiles concurrently with S-, X- and Ku-Band propagation measurements along a 26-km path. Using existing surface-layer bulk models, profiles of the gradient of modified refractivity were computed from the buoy data at one level and compared with the actual values obtained from the kite and the buoy. The bulk estimates did not agree well with the buoy data within the lowest 5 m. The kite and buoy data did not show the strong gradients just above the surface that were expected from theory. This same effect was noted when the kite experiment was repeated over much colder water near San Diego, CA. A refractive model was not able to forecast the variability of measured RF propagation characteristics when driven with the merged kite and buoy data. Using bulk estimates did result in some forecast skill.				
14. SUBJECT TERMS RF propagation, boundary layer, refractivity, bulk			15. NUMBER OF PAGES 66	
			16. PRICE CODE	
17. SECURITY CLASSIFICATION OF REPORT Unclassified	18. SECURITY CLASSIFICATION OF THIS PAGE Unclassified	19. SECURITY CLASSIFICATION OF ABSTRACT Unclassified	20. LIMITATION OF ABSTRACT UL	

THIS PAGE INTENTIONALLY LEFT BLANK

Approved for public release; distribution is unlimited.

VARIABILITY OF REFRACTIVITY IN THE SURFACE LAYER

Deborah L. Mabey
Lieutenant, United States Navy
B.S., Clemson University, 1995
M.S., University of Charleston, S. C., 1999

Submitted in partial fulfillment of the
requirements for the degree of

**MASTER OF SCIENCE IN METEOROLOGY AND PHYSICAL
OCEANOGRAPHY**

from the

**NAVAL POSTGRADUATE SCHOOL
June 2002**

Author: Deborah L. Mabey

Approved by: Kenneth L. Davidson
Thesis Advisor

Peter Guest
Co-advisor

Carlyle Wash
Chairman, Department of Meteorology

THIS PAGE INTENTIONALLY LEFT BLANK

ABSTRACT

The author and members of the Boundary Layer Studies Group collected atmospheric surface layer profile properties affecting RF propagation during the Roughness and Evaporation Duct experiment off the windward coast of Oahu. We measured temperature, humidity and pressure profiles from the surface and up to 100 m by multi-level buoy-mounted sensors and a rawinsonde attached to a kite flown from a small vessel. We obtained the profiles concurrently with S-, X- and Ku-Band propagation measurements along a 26-km path. Using existing surface-layer bulk models, profiles of the gradient of modified refractivity were computed from the buoy data at one level and compared with the actual values obtained from the kite and the buoy. The bulk estimates did not agree well with the buoy data within the lowest 5 m. The kite and buoy data did not show the strong gradients just above the surface that were expected from theory. This same effect was noted when the kite experiment was repeated over much colder water near San Diego, CA. A refractive model was not able to forecast the variability of measured RF propagation characteristics when driven with the merged kite and buoy data. Using bulk estimates did result in some forecast skill.

THIS PAGE INTENTIONALLY LEFT BLANK

TABLE OF CONTENTS

I.	IMPORTANCE OF MODIFIED REFRACTIVITY IN THE SURFACE LAYER.....	1
A.	INTRODUCTION.....	1
B.	BACKGROUND	1
1.	Index of Refraction, Refractivity and Modified Refractivity	1
2.	Monin-Obukhov Similarity (MOS) Theory and the Bulk Method	3
C.	IMPORTANCE TO NAVAL APPLICATIONS.....	4
1.	Three Types of Ducts	4
a.	<i>Elevated Ducts</i>	5
b.	<i>Surface-based Ducts</i>	5
c.	<i>Evaporation Ducts</i>	6
2.	A Specific Example: SPY-1 Radar	8
II.	DATA COLLECTION	9
A.	WARM WATER (RED) EXAMPLES	9
1.	Naval Postgraduate School (NPS) Buoy.....	9
2.	Radiosonde Attached to Kite Flown From Vessel Wailoa	9
3.	S-, X- and Ku-Band Propagation Data	12
B.	COLD WATER EXAMPLES.....	12
1.	Weather Station Aboard Small Boat	12
2.	Radiosonde Attached to Kite Flown From Small Boat	13
III.	DATA ANALYSIS	15
A.	DATA PREPARATION.....	15
1.	Buoy and Propagation Data	15
2.	Kite Data	15
a.	<i>Initial Editing</i>	15
b.	<i>Height Adjustment</i>	15
3.	Averaging Period Selection	16
B.	ENVIRONMENTAL DATA ANALYSIS	18
1.	Smoothed Data Results.....	18
2.	Bulk Method Results	23
3.	Summary of Environmental Profiles	23
IV.	PROPAGATION PREDICTIONS.....	27
A.	AREPS CONFIGURATION.....	27
B.	WARM-WATER RESULTS	28
C.	COLD WATER RESULTS.....	36
V.	SUMMARY.....	39
A.	PRESENT STUDY LIMITATIONS	39
1.	Kite-borne radiosonde	39
a.	<i>Vaisala RS-80 radiosonde</i>	39

<i>b.</i>	<i>Data Matching</i>	40
2.	Averaging Period Selection	41
3.	Profile Smoothing	41
4.	Propagation Prediction and Measurement.....	41
<i>a.</i>	<i>Measured Propagation Loss</i>	41
<i>b.</i>	<i>Variability of Refractivity Conditions Along the Propagation Path</i>	42
B.	CONCLUSIONS	42
1.	Profiles of Modified Refractivity	42
2.	Propagation Predictions	43
	LIST OF REFERENCES.....	45
	INITIAL DISTRIBUTION LIST	47

LIST OF FIGURES

Figure 1.	Comparison of refractivity (N) and modified refractivity (M) illustrating how useful modified refractivity is in identifying the transition from superrefraction to trapping (ducting). This height is marked by an asterisk and is called the duct height. In this specific example, the duct is due to a strong humidity gradient near the ocean surface and is called an evaporation duct (and therefore the duct height is call the evaporation duct height).....	2
Figure 2.	A comparison of the profile of M with respect to z for three types of ducts.....	5
Figure 3.	Effect of surface-based ducting on propagation loss.	6
Figure 4.	Effect of evaporation ducting on propagation loss.	7
Figure 5.	Propagation loss (dB) versus distance (km) for an environment with an evaporation duct height of 20 m and an antenna height of 10 m. Top left: L-Band (1 GHz); Top Right: S-Band (3 GHz); Bottom Left: X-Band (10 GHz); Bottom Right: Ku-Band (18 GHz). The color scheme is the same for all four panels. Red: <110 dB; Yellow: 110-115 dB; Magenta: 115-120 dB; Blue: 120-125 dB; Green: 125-130 dB, etc.....	8
Figure 6.	Simple diagram of kite flying configuration. NOT TO SCALE.	10
Figure 7.	Left: Close up view of kite rigging. Right: Safety snap swivel (and drawing) showing terms used to describe attachment.....	11
Figure 8.	Radiosonde pressure record showing manual selection of starting and stopping points for each kite up/down.	16
Figure 9.	Summary record showing justification for subjective averaging period selection. Blue dots represent data collected by the kite-borne radiosonde. Black dots represent data collected by the NPS buoy. Red dots represent data collected from onboard R/V Wailoa (used for comparison/corroboration only). Blue vertical lines show averaging period starting and stopping points.	17
Figure 10.	Summary record from cold-water experiment showing extreme ship's envelope contamination, as characterized by positive spikes in the temperature record.....	18
Figure 11.	Profiles of temperature, specific humidity and modified refractivity versus height (log scale). Black circles are buoy data. Blue circles are kite-borne radiosonde data. Bars associated with blue circles represent plus and minus one standard deviation. Blue circles without associated bars are averages of less than ten data points. Solid lines are bulk profiles. The black solid line is computed from the 4.08-meter buoy data. The blue solid line is computed from the 19.5-meter kite-borne radiosonde data.	20
Figure 12.	Left panel shows actual kite-borne radiosonde data (blue circles) and buoy data (black circles) with quadratic functions fit to them. Right panel shows the same buoy data with the adjusted kite-borne radiosonde data (magenta circles).	21

Figure 13.	An example (linear height scale on the right, log on the left) of a case when the bulk profile from the buoy data (black line, procedure described below) and the smoothed profile from the kite-borne radiosonde data merged with the buoy data (magenta line, procedure described above) match extremely well above 3.5 m.	22
Figure 14.	An example (linear height scale on the right, log on the left) of a case when the bulk profile from the buoy data (black line, procedure described below) and the smoothed profile from the kite-borne radiosonde data merged with the buoy data (magenta line, procedure described above) match poorly at all levels. Cases like this are rare.	22
Figure 15.	Blue lines represent the mean difference between the first order approximations of dM/dz (45 averaging periods). Red lines represent plus and minus two standard deviations. Top left panel is from five to 50 m. Top right panel is from one to five m. Bottom panel is from the surface to one m. Asterisks are used for the 0.05-meter values.	24
Figure 16.	S-Band propagation factor versus distance for September 1, 2001 from 1933 to 1955 UTC. The vertical axis of each plot is propagation factor (propagation loss predicted minus propagation loss in free space, measured in dB). The horizontal red dashed line represents a propagation factor of zero; propagation loss equal to free space propagation loss. The horizontal axis of each plot is distance measured in km. The vertical red dashed line represents the length of the propagation path during the RED experiment. The black line represents propagation factor based on the bulk profile of modified refractivity. The magenta line represents propagation factor based on the smoothed profile from the merged buoy and kite data. The blue line represents propagation factor based on the standard atmosphere. The green dots represent measured values of propagation loss for the appropriate frequency, antenna height, and time period (converted to propagation factor by subtracting the appropriate propagation loss in free space). The top panel is for the higher antenna and the bottom panel is for the lower antenna.	29
Figure 17.	As above, but for X-Band.	30
Figure 18.	As above, but for Ku-Band.	30
Figure 19.	As in figure 16, but for September 6, 2001 from 1910 to 1925.	31
Figure 20.	As above, but for X-Band.	31
Figure 21.	As above, but for Ku-Band.	32
Figure 22.	Summary of predicted versus measured propagation loss for the high antenna S-Band. Black circles represent predictions from bulk profiles. Magenta asterisks represent predictions from smoothed profiles of merged kite and buoy data.	33
Figure 23.	As above, but for the low antenna S-Band.	33
Figure 24.	As above, but for the high antenna X-Band.	34
Figure 25.	As above, but for the low antenna X-Band.	34
Figure 26.	As above, but for the high antenna Ku-Band.	35
Figure 27.	As above, but for the low antenna Ku-Band.	35

Figure 28. Time series showing propagation measurement availability (blue dots) and kite-borne radiosonde averaging periods (red vertical lines).42

THIS PAGE INTENTIONALLY LEFT BLANK

LIST OF TABLES

Table 1.	Classes of Refraction.....	2
Table 2.	Kite-borne radiosonde sensors.....	12
Table 3.	Mean and standard deviation of the difference between the values and gradients of modified refractivity of bulk and smoothed profiles based on 45 averaging periods. The information in the two right-hand columns is the same as that presented in Fig 15.....	25
Table 4.	AREPS parameters.....	27
Table 5.	Comparison of variability and predictive capability of bulk and merged profiles of modified refractivity.....	36

THIS PAGE INTENTIONALLY LEFT BLANK

ACKNOWLEDGMENTS

To Anthony, for all the afternoons I could not make it to the playground and for all the evenings I did not come home in time for dinner.

THIS PAGE INTENTIONALLY LEFT BLANK

I. IMPORTANCE OF MODIFIED REFRACTIVITY IN THE SURFACE LAYER

A. INTRODUCTION

The vertical gradient of the modified index of refraction (or modified refractivity), M , is important for understanding the propagation of UHF, VHF and microwave frequencies in the troposphere. M depends on three atmospheric parameters: pressure (p), temperature (T), and the partial pressure of water vapor (e). Gradients of humidity near the surface over ocean regions usually causes energy from radio waves at frequencies greater than approximately 3 GHz to be trapped in the atmospheric surface layer, a phenomenon called evaporation ducting. This leads to significant increases in propagation distance compared to a standard atmosphere, which does not have a strong surface humidity gradient. Since these gradients cannot normally be measured precisely near the surface, bulk methods (Fairall, et. al, 1996) based on single level and surface measurements are used to approximate the profile of M . The purposes of this study are: 1) to evaluate bulk methods by measuring profiles of p , T and e directly using a buoy and a kite flown from a mobile platform; 2) to evaluate the impact of differences between the bulk and directly-measured profiles on radio frequency propagation using the Advanced Refractive Effects Prediction System (AREPS) program; 3) to compare AREPS predictions based on bulk and directly-measured profiles with observed loss values and 4) to encourage future studies aimed at resolving significant differences between the propagation predictions based on bulk and directly-measured profile data and also the direct RF loss observations.

B. BACKGROUND

1. Index of Refraction, Refractivity and Modified Refractivity

The index of refraction, n , of the atmosphere determines the phase speed of electromagnetic waves passing through it (and therefore also the different phase speeds along an individual wave front). The value of n is very close to 1, so refractivity (N) is used instead, where $N=(n-1)\times 10^6$. The actual value of N is not important in most applications, but rather the gradient of N with respect to height, dN/dz . Table 1 illustrates the relationship between dN/dz and the distance to the horizon.

Class	dN/dz	Propagation Range
Subrefraction	$dN/dz > 0 \text{ km}^{-1}$	decreased
Normal	$0 \text{ km}^{-1} > dN/dz > -79 \text{ km}^{-1}$	normal
Superrefraction	$-79 \text{ km}^{-1} > dN/dz > -157 \text{ km}^{-1}$	increased
Trapping (ducting)	$dN/dz < -157 \text{ km}^{-1}$	greatly increased

Table 1. Classes of Refraction

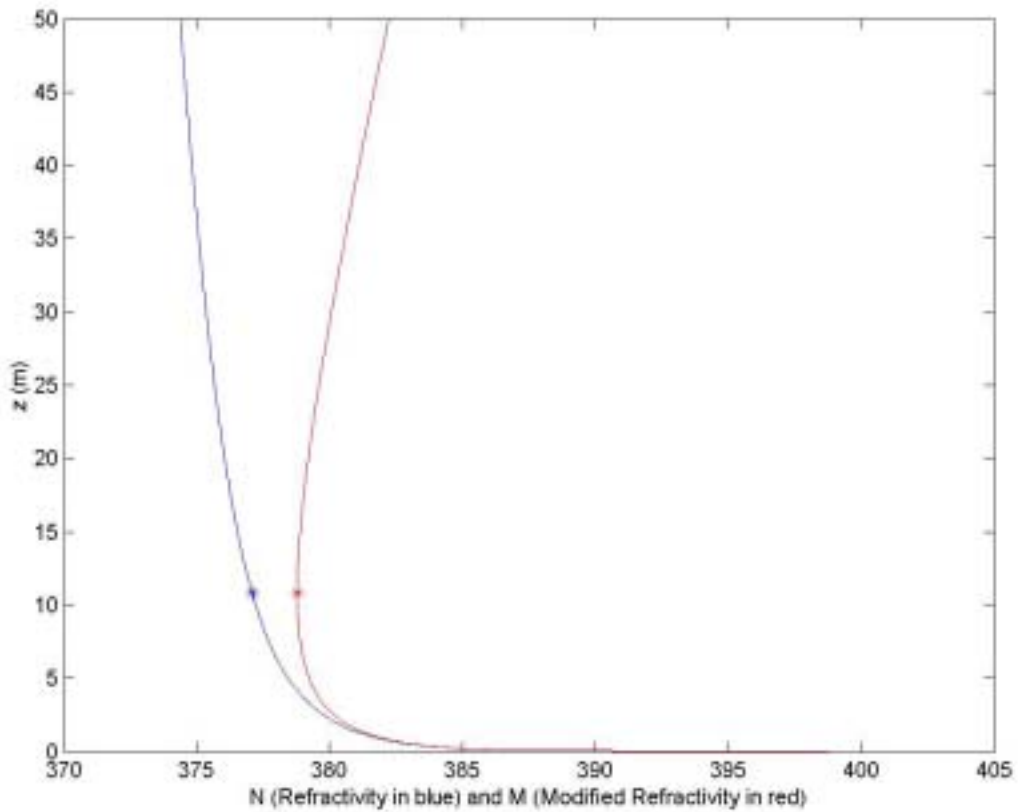


Figure 1. Comparison of refractivity (N) and modified refractivity (M) illustrating how useful modified refractivity is in identifying the transition from superrefraction to trapping (ducting). This height is marked by an asterisk and is called the duct height. In this specific example, the duct is due to a strong humidity gradient near the ocean surface and is called an evaporation duct (and therefore the duct height is called the evaporation duct height).

Note that it is difficult to identify regions of ducting from a simple visual inspection of a profile of N (Fig 1, blue). This problem is alleviated by the use of M (Fig 1, red), where $M=N+(0.157 \text{ m}^{-1})z$ and z is the height above the surface in m. Ducting

will occur when $dM/dz < 0$, making it easier to visualize regions of ducting. If ducting occurs due to a humidity gradient immediately above the surface, it is deemed an evaporation duct because surface evaporation creates the strong humidity gradient responsible for the ducting. The level at which $dM/dz = 0$ is the evaporation duct height. Sea surface temperature has an important role in evaporation duct characteristics because the vapor pressure at the surface is a strong function of water temperature. The value of M is a function of pressure, air temperature and vapor pressure (the latter derived from relative humidity and air temperature):

$$M = 77.6 \frac{p}{T} - 5.6 \frac{e}{T} + 375000 \frac{e}{T^2} + 0.157z$$

In a typical operational situation, direct profile measurements of e , T and p , and therefore M , are not possible and we must use bulk methods to estimate the profiles. Using the equation below, the partial derivatives of N as well as the variation of pressure with height are assumed to be constant.

$$\frac{dM}{dz} = \frac{\partial N}{\partial q} \frac{\partial q}{\partial z} + \frac{\partial N}{\partial T} \frac{\partial T}{\partial z} + \frac{\partial N}{\partial p} \frac{\partial p}{\partial z} + 0.157 \text{ m}^{-1}$$

This leaves only the vertical gradients of T and q to be determined, where q is the specific humidity, a parameter closely related to e . This thesis uses the bulk method described in the following section to estimate these gradients from measurements at a single airflow level and at the surface.

2. Monin-Obukhov Similarity (MOS) Theory and the Bulk Method

Monin-Obukhov theory states that the vertical gradients of temperature ($\frac{\partial T}{\partial z}$) and specific humidity ($\frac{\partial q}{\partial z}$) in the surface layer depend on scaling parameters that are related to the turbulent vertical fluxes of momentum, sensible heat and latent heat (moisture). When turbulent fluxes are not measured directly, the Monin-Obukhov scaling parameters can be determined using measurements of temperature (T_s) at the surface (humidity at a sea water surface is assumed to be 98% of the pure water saturation humidity value), as well as temperature, humidity and wind speed at some reference height, z , which must be near (within approximately 20 m of) the surface. Other important parameters, which are

based on empirically derived functions and constants, are the MOS stability function (ψ) and roughness length (z_{oT}). Because the stability function (the form of which is not shown) is itself a function of the MOS scaling parameters, the following equations must be solved by an iterative procedure that usually converges after about five cycles. The example equations are for temperature, but similar equations apply for surface layer humidity and wind speed profiles. Values subscripted with asterisks are scaling parameters, κ is the von Karman constant (0.4), g is the acceleration of gravity, and L is the Obukhov length scale.

$$T_* = (T_z - T_s) \kappa \left[\ln \left(\frac{z}{z_{oT}} \right) - \psi_T(\xi) \right]^{-1}$$

$$\xi = \frac{z}{L}$$

$$L = \frac{T_v u_*^2}{\kappa g (T_* + 0.61 T q_*)}$$

Once the scaling parameters are determined, the gradients can be calculated using equations similar to the equation for the temperature gradient, $\frac{\partial T}{\partial z} = \frac{T_*}{\kappa z} \Phi \left(\frac{z}{L} \right)$, where Φ is a stability function determined experimentally over land (Fairall, et. al, 1996 and Davidson, 2002). We call the time-averaged surface and reference height variables bulk parameters and thus the profiles of T , q and M derived in this manner are called bulk profiles.

C. IMPORTANCE TO NAVAL APPLICATIONS

1. Three Types of Ducts

Ducts occur only when the gradient of M is negative. We can easily visualize the location of a duct on plots of M versus z by drawing a vertical line down from a local minimum of M . The duct exists in the region from the M minimum to where the vertical line intersects either the M profile or the surface. There are three types of ducts: elevated ducts, surface-based ducts and evaporation ducts (Fig 2). The scaling equations just described apply only to evaporation ducts.

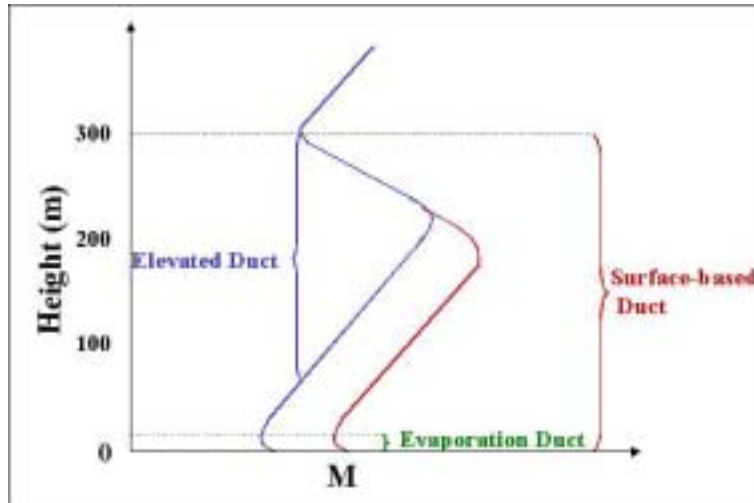


Figure 2. A comparison of the profile of M with respect to z for three types of ducts.

a. *Elevated Ducts*

An elevated duct occurs when a local minimum of M has a value greater than the value of M at the surface. Elevated ducts are caused by temperature and/or humidity inversions (increases in temperature and decreases in specific humidity with height). These inversions are often associated with large high-pressure systems and are due to the subsidence of warm, dry air over cool, moist air. Of the three types of ducts, elevated ducts have the least effect on tactical applications. (O'Connor, 2001)

b. *Surface-based Ducts*

Surface-based ducts have similar profiles of M with respect to z , except that the value of M at the elevated local minimum is smaller than the value of M at the surface. Over the ocean, surface-based ducts often occur when warm, dry air is advected over cool water. Surface-based ducts significantly affect propagation by creating an alternating pattern of skip zones (Fig 3). They only occur over the world's oceans about 10% of the time, but they can be much more frequent in certain locations and seasons. (O'Connor, 2001)

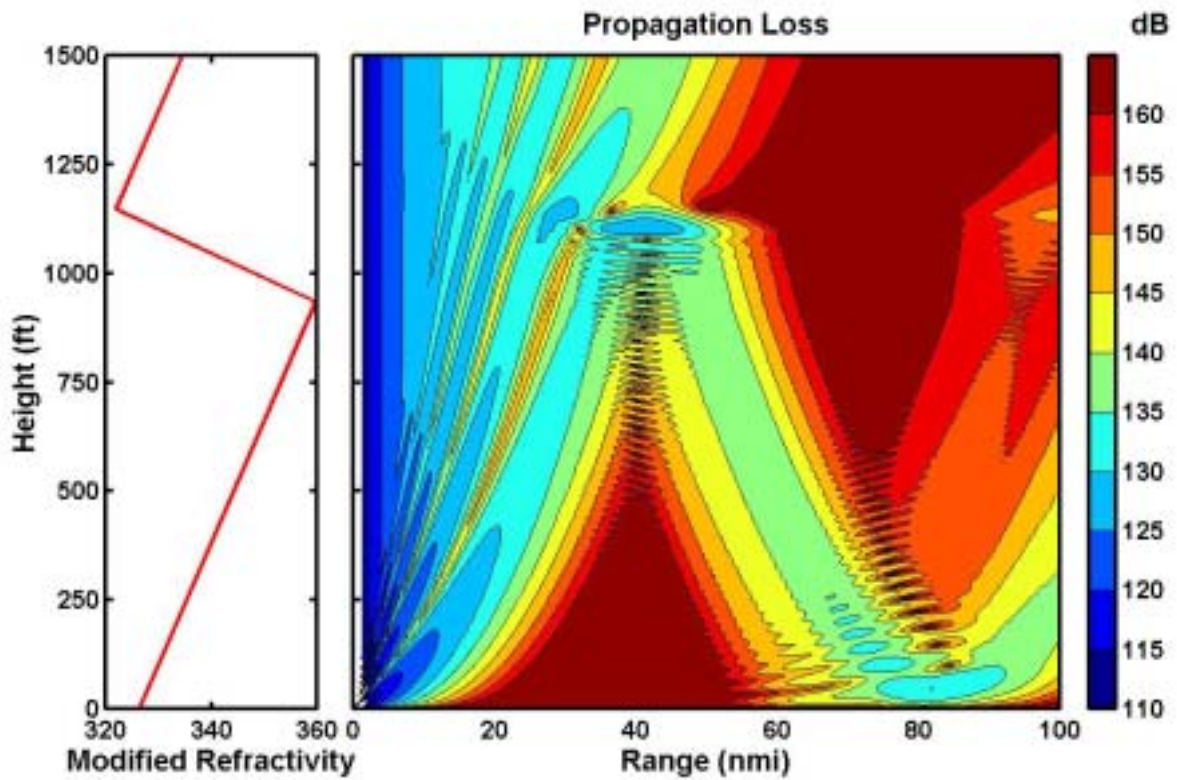


Figure 3. Effect of surface-based ducting on propagation loss.

c. Evaporation Ducts

Over the ocean, a strong gradient of humidity above the surface leads to an evaporation duct. Unlike surface-based ducting, which occurs infrequently, evaporation ducts are almost always present over the ocean. Evaporation ducts significantly affect propagation by keeping radiation near the surface, thus extending the propagation range and filling in skip zones created by surface-based ducts (Fig 4).

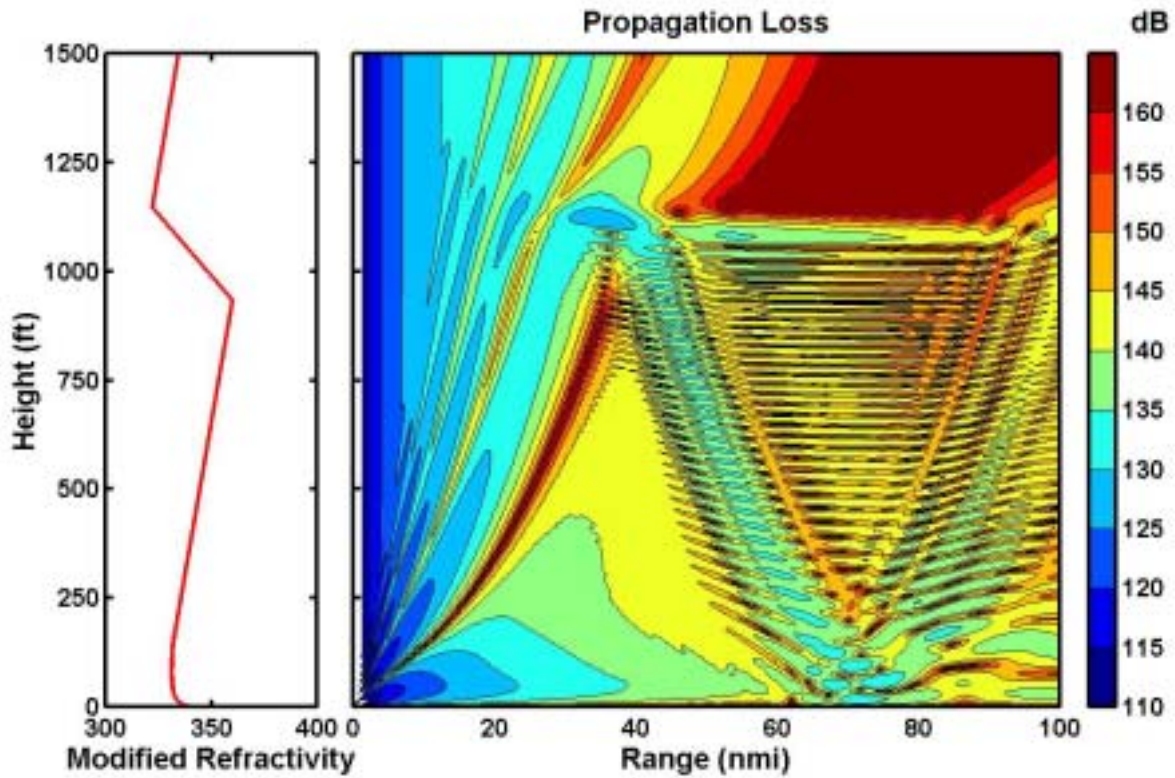


Figure 4. Effect of evaporation ducting on propagation loss.

The effect of evaporation ducting is dependent on frequency. Fig 5 shows propagation loss for L-Band, S-Band, X-Band and Ku-Band frequencies for an evaporation duct height of 20 m and an antenna height of 10 m. The L-Band frequency (1 GHz) is relatively unaffected by evaporation ducting. The S-Band frequency (3 GHz) shows extended ranges at all heights, but especially near the evaporation duct height. The X-Band frequency (10 GHz) exhibits decreased propagation loss centered on the antenna height while the Ku-Band frequency (18 GHz) shows decreased loss near the antenna height as well as near the evaporation duct height. These results are specific to the environment, antenna height and frequencies used, but do serve to illustrate the frequency-dependent nature of propagation in the presence of an evaporation duct.

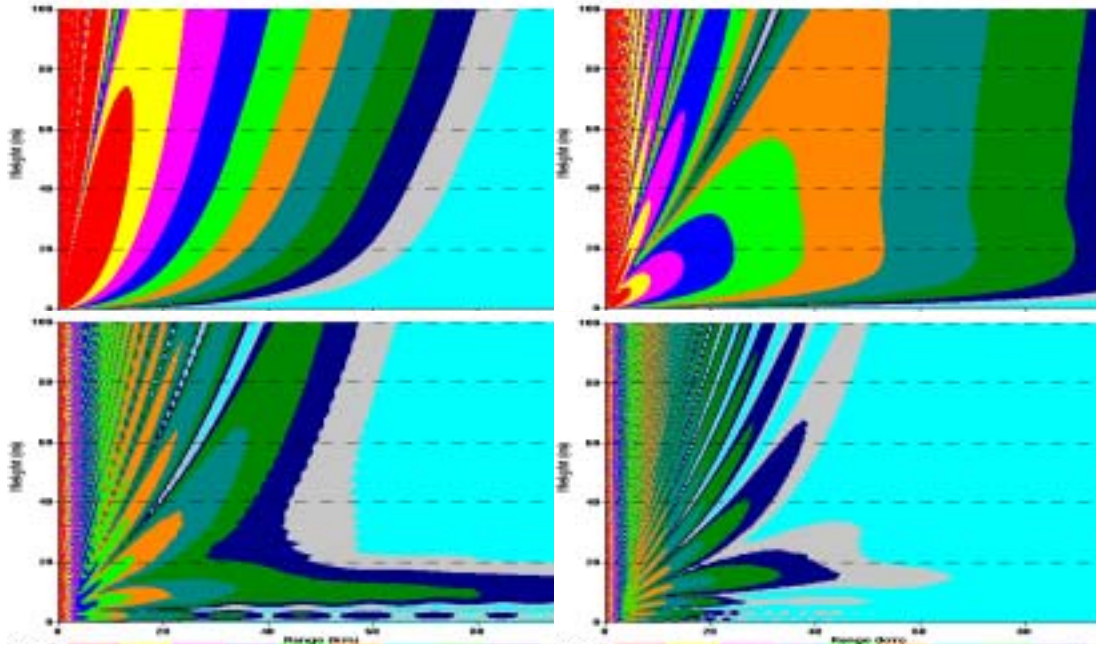


Figure 5. Propagation loss (dB) versus distance (km) for an environment with an evaporation duct height of 20 m and an antenna height of 10 m. Top left: L-Band (1 GHz); Top Right: S-Band (3 GHz); Bottom Left: X-Band (10 GHz); Bottom Right: Ku-Band (18 GHz). The color scheme is the same for all four panels. Red: <110 dB; Yellow: 110-115 dB; Magenta: 115-120 dB; Blue: 120-125 dB; Green: 125-130 dB, etc.

2. A Specific Example: SPY-1 Radar

The SPY-1A, B, B(V), D and D(V) radars all use S-Band frequencies, and future generations of the SPY radar may operate at even higher frequencies. (Kimbrell, 2001) To take full advantage of the capabilities of the SPY-1 radar, operators must account for changing near-surface refractivity conditions. (Sanabia, 2000)

II. DATA COLLECTION

A. WARM WATER (RED) EXAMPLES

The Roughness and Evaporation Duct (RED) experiment was designed in response to the recognition that propagation models seem to underestimate loss at high frequencies over water surfaces in the presence of high winds. This could be due to problems with current atmospheric boundary layer (ABL) theories or surface scattering theories in the presence of high winds and rough surfaces. The purpose of the experiment was to relate the effect of both the ABL and ocean surface roughness to high frequency electromagnetic propagation.

To that end, ABL and ocean surface data from two sources, as well as propagation data, were collected from August to September 2001 off the windward coast of Oahu, Hawaii during the RED experiment. The Oahu location was chosen because the warm surface in the trade wind region produces strong evaporation ducts and rough surfaces are often present. This thesis will analyze the environmental data and compare it to the propagation measurements in order to evaluate atmospheric effects on propagation.

1. Naval Postgraduate School (NPS) Buoy

The NPS buoy collected atmospheric surface layer and ocean surface data continuously at a one second interval from August 22, 2001 0240 UTC until September 18, 2001 1554 UTC. The buoy collected pressure data at 0.39 m above the surface, wind speed and wind direction data at 4.15 m above the surface, and air temperature and relative humidity data at 0.71, 1.04, 2.06 and 4.08 m above the surface. Although the buoy collected sea surface temperature measurements at 1.2 m below the surface and at the surface using a floating thermistor, this thesis will only use infrared sea surface temperature since it is the most useful measurement for use in calculating bulk profiles.

2. Radiosonde Attached to Kite Flown From Vessel Wailoa

The Boundary Layer Studies Group at NPS designed a kite-borne radiosonde system (Fig 6) to measure profiles of the refractivity-determining parameters; pressure, temperature and vapor pressure; from near the surface (<1 m) to the top of the surface layer (approximately 100 m).

Depending on wind speed, we attached an approximately ten-meter length of 50-pound test kite string to either a four-foot or six foot nylon delta kite. A swivel affixed by its free solid ring was at the end of this length of kite string (see Fig 7). We attached the safety snap of another swivel through the same free solid ring of the first swivel. The free solid ring of the second swivel was attached to approximately 500 feet of 50-pound test kite string. The 500 feet of kite string was on a reel attached to a salt-water fishing rod that was secured to the side of the boat. With all this rigging in place, we would launch the kite and allow it to fly only far enough from the boat so the swivels were still accessible from the deck.

During the process of rigging and launching the kite, we prepared and activated a Vaisala RS-80 radiosonde for manual launch. We unwound the top portion of string from the radiosonde suspension string unwinder and detached it from the remaining length of string. The loose end was formed into a loop. We attached this loop to the safety snap of the swivel already tied to the string leading to the kite while the kite was still in the air.

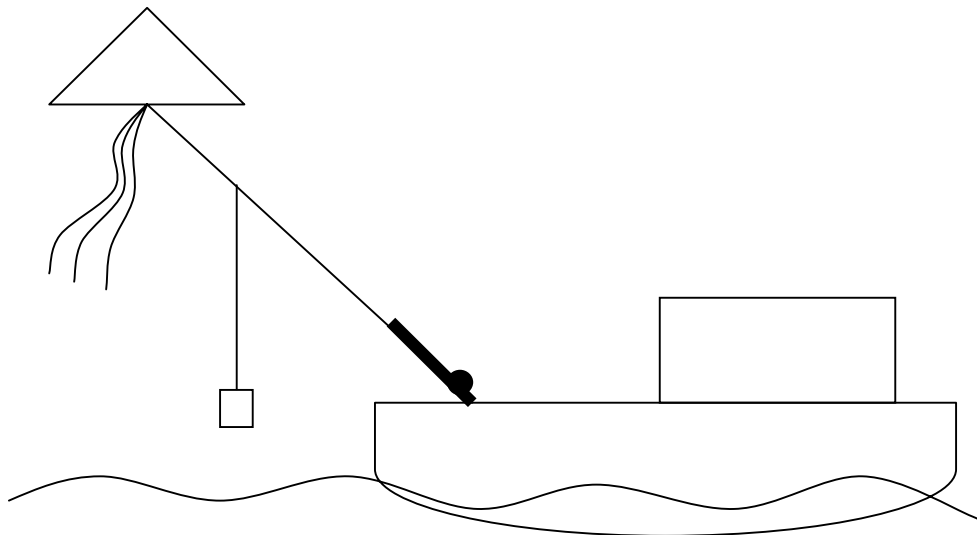


Figure 6. Simple diagram of kite flying configuration. NOT TO SCALE.

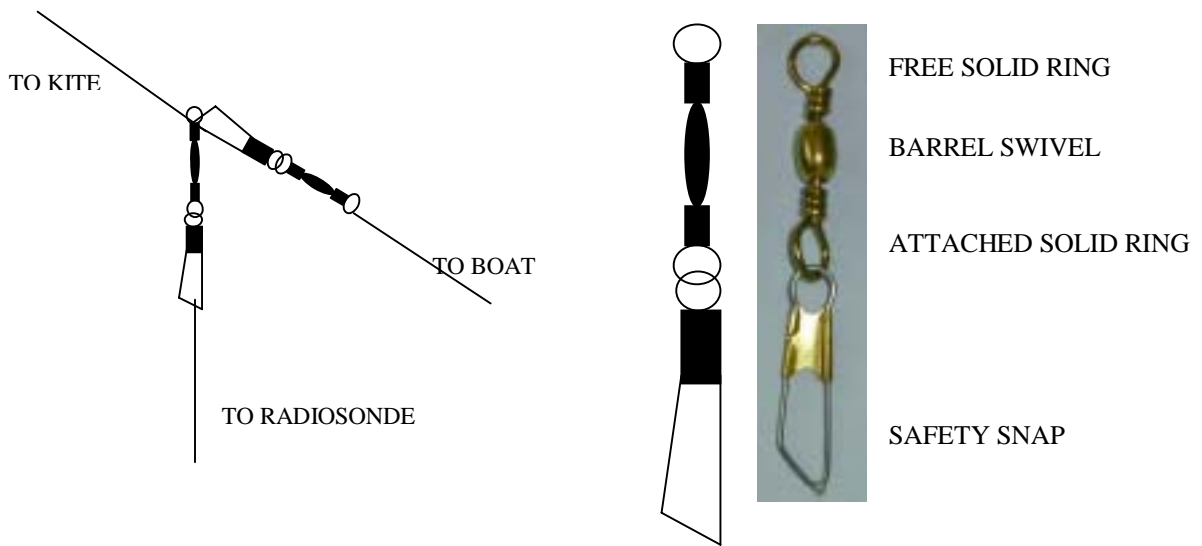


Figure 7. Left: Close up view of kite rigging. Right: Safety snap swivel (and drawing) showing terms used to describe attachment.

With the drag on the reel turned off, we applied pressure directly to the side of the reel by hand to control the rate at which the kite string spooled out. We did this in such a manner that the radiosonde moved horizontally away from the ship while maintaining a height above the sea surface of approximately one m. In order for this to be possible with a six-foot delta kite, it was necessary to have a steady relative wind speed of approximately four meters per second. Once the steady relative wind speed exceeded ten meters per second, we would switch from a six-foot delta kite to a four-foot delta kite. This was to keep from breaking the kite string and also to reduce to a reasonable level the human labor required to reel the in kite.

Once the kite-borne radiosonde had reached a distance of approximately 50 to 100 m away from the ship, we allowed the kite and radiosonde to rise slowly by slightly decreasing the pressure applied to the side of the reel. When the kite reached a height of approximately 100 m, we restored full drag to the reel. This would cause the kite to rise very quickly. The kite continued to rise as we reeled the string in and would then decrease in height after reaching some critical angle with the horizontal based on the relative wind speed. We reeled the kite in until the radiosonde was approximately one m from the side of the ship. After a brief pause, we repeated the process until the time limit

of data collection (two hours) was reached. In this manner, we completed approximately fifteen to 25 up and down kite profiles during each two-hour data collection session.

The Vaisala RS-80 radiosonde transmitted measured values of temperature, pressure and vapor pressure every two seconds.

	Type of Sensor	Range	Accuracy	Resolution	Response/Lag Time
Pressure	Capacitive aneroid	1060 to 3 hPa	0.5 hPa	0.1 hPa	
Temperature	Capacitive bead	-90 to 60 °C	0.2 °C	0.1 °C	2.5 seconds
Humidity	Thin film capacitor	0 to 100%	2%	1%	1 second

Table 2. Kite-borne radiosonde sensors.

3. S-, X- and Ku-Band Propagation Data

Two antennas at different heights above the surface transmitted radio waves at three frequencies, S-Band (2.975 GHz), X-Band (9.7 GHz) and Ku-Band (17.7 GHz). The transmitting antennas were aboard R/P FLIP and at nominal heights above sea level of 12.62 and 4.88 m. The receiving antenna was on shore, 25.77 km away, at a nominal height above sea level of 4.73 m. The RED scientists collaborating with the BLSG measured propagation loss on a five-minute cyclic basis for each of the six frequency/antenna height combinations. The propagation data were averaged over the five-minute collection periods, resulting in one averaged value for each frequency/antenna height combination every thirty minutes.

B. COLD WATER EXAMPLES

The BLSG collected data from two sources during November and December 2001 near the Channel Islands west of San Diego, California.

1. Weather Station Aboard Small Boat

The weather station sampled meteorological data continuously at a one second interval from November 30, 2001 1459 UTC until December 5, 2001 0148 UTC (with a gap from December 2, 2001 2353 UTC until December 3, 2001 1432 UTC). These data were then averaged over one-minute intervals. The station collected pressure data at 5.92 m above the surface, wind speed and wind direction data at 6.76 m above the surface and

air temperature and relative humidity data at 5.66 m above the surface. The station also collected infrared sea surface temperature.

2. Radiosonde Attached to Kite Flown From Small Boat

The procedure was identical to that described for the warm water example.

THIS PAGE INTENTIONALLY LEFT BLANK

III. DATA ANALYSIS

A. DATA PREPARATION

1. Buoy and Propagation Data

As mentioned previously, buoy and propagation data were averaged over one-minute and five-minute periods, respectively. Also, they had already been examined for bad data and had such values either removed or corrected. For these reasons, this thesis used both the buoy and propagation data in the form in which they were received; only the kite data were edited and corrected.

2. Kite Data

a. Initial Editing

The kite data had to be edited and formatted into an acceptable form for analysis and display. Bad data (generally due to receiving a signal from another radiosonde) and missing data were removed.

b. Height Adjustment

Although we collected height data from the radiosonde receiving system, it was unreliable because it was based on the integrated hydrostatic balance assumption using radiosonde measured temperature and pressure. For this assumption to be valid, surface pressure would have to remain constant during the 2-hour data collection periods, but it did not. When attempts to adjust height based on the surface pressure transient measured by the ship's weather station and the buoy were both unsuccessful, another approach was taken.

We assumed that the kite reached a minimum elevation of one m each time it was allowed to leave the ship. This required subjective interpretation of the pressure record to determine the points where the kite left the ship and where it returned (see Fig 8 below). During each of these periods (which lasted approximately five minutes), the minimum height was adjusted to one m and all other heights were adjusted by the same amount.

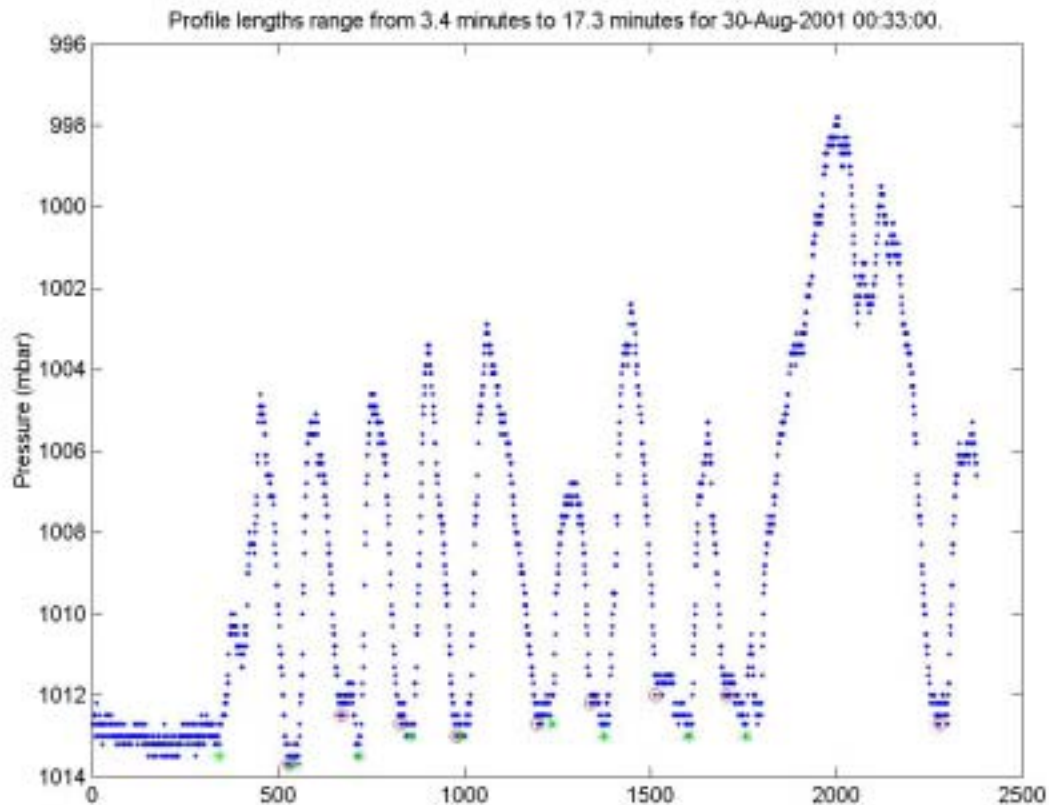


Figure 8. Radiosonde pressure record showing manual selection of starting and stopping points for each kite up/down.

3. Averaging Period Selection

Once the appropriate kite data height adjustment had been made, the whole record was divided into averaging periods using all available data. This was done subjectively by examining the buoy data and determining when conditions were approximately constant. The averaging periods were approximately 20 to 40 minutes in duration.

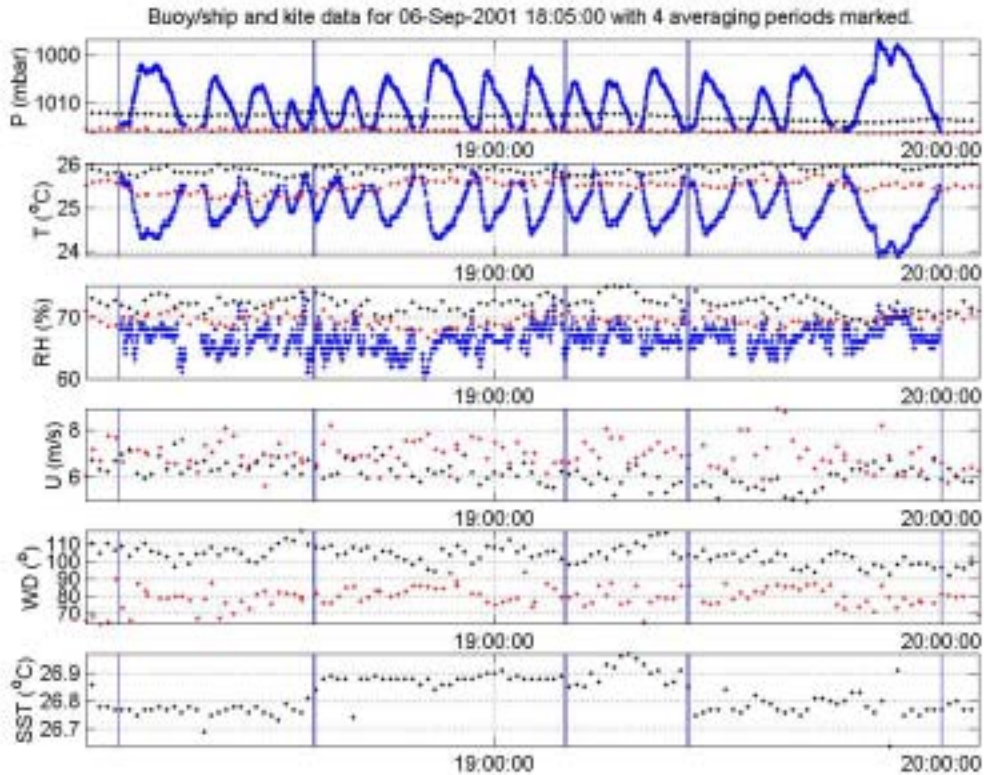


Figure 9. Summary record showing justification for subjective averaging period selection. Blue dots represent data collected by the kite-borne radiosonde. Black dots represent data collected by the NPS buoy. Red dots represent data collected from onboard R/V Wailoa (used for comparison/corroboration only). Blue vertical lines show averaging period starting and stopping points.

These time series were also useful in determining whether the low-level measurements made by the kite-borne radiosondes were contaminated by the ship's envelope. The data on Fig 9 showed little such contamination. As an extreme counterexample, the data on Fig 10 clearly showed the effect of the ship's envelope every time the kite is raised and lowered. The signature of the ship's envelope is most noticeable in the temperature signal, where temperature increases two to three degrees C as the kite is released from and reeled in toward the ship. This effect can also be recognized by a decrease in humidity. (This is an example from the cold-water experiment, which used a much larger ship than the warm-water experiment.)

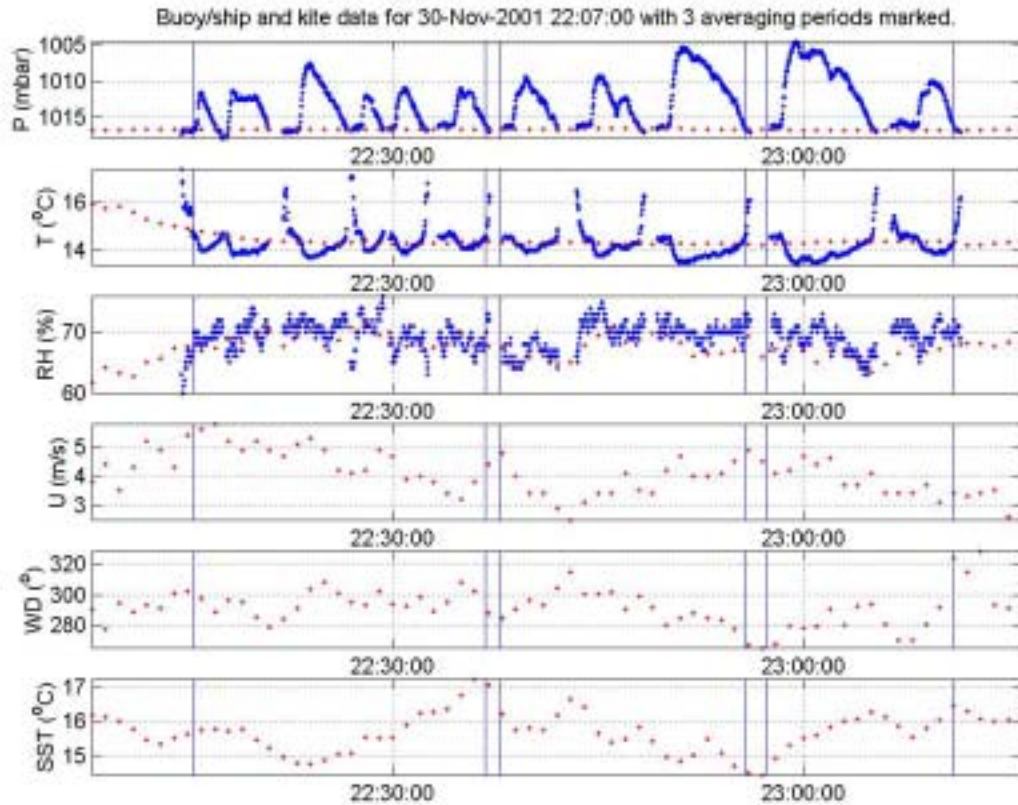


Figure 10. Summary record from cold-water experiment showing extreme ship's envelope contamination, as characterized by positive spikes in the temperature record.

B. ENVIRONMENTAL DATA ANALYSIS

For each averaging period, the analysis procedure used two approaches to ascertain a representative profile of refractivity. One was based on model calculations rather than direct profile measurements.

1. Smoothed Data Results

The analysis grouped kite data within each averaging period into height bins for averaging. Since the height resolution was only to the nearest m, below 32 m each bin included measurements from only two levels and the averaged value was assigned to the mid-level height. For example, the 1 m and 2 m levels were grouped into the 1.5 m bin, the 3 m and 4 m levels were grouped into the 3.5 m bin, etc. From 35 to 100 m, the bins contained 5-meter levels. For example, the 35 m bin included the 33, 34, 35, 36 and 37-

meter levels. The procedure used Monin-Obukhov scaling parameters based on the TOGA-COARE model of Fairall, et al. (1996) to produce a bulk profile from each data point, and interpolate refractivity for each point to the midpoint level of its appropriate bin. These interpolated refractivity values were then averaged to create 30 bin-averaged data points at two m spacing from 1.5 up to 31.5 m and five m spacing from 35 up to 100 m. For example, a bulk profile would be created using measurements from 39 m. The 40 m refractivity from that bulk profile would be used as part of the average for the 40 m bin.

The analysis used buoy humidity and temperature data at 0.71 m, 1.04 m, 2.06 m and 4.08 m and buoy pressure data at 0.39 m (adjusted to the appropriate level to match with temperature and humidity measurements) to calculate refractivity values using the equation $M = 77.6 \frac{P}{T} - 5.6 \frac{e}{T} + 375000 \frac{e}{T^2} + 0.157z$. In a majority of cases, the bin averaged M values at the lowest two levels (1.5 and 3.5 m) from the kite data were too low so the profiles did not exhibit the strong humidity gradient that was expected. This feature and the fact that these low level values were not in agreement with the buoy measurements suggested that there was an error in the lowest level kite values. For this reason, this study did not include the 1.5 m and 3.5 m bins in any regression fits (see Fig 11 below).

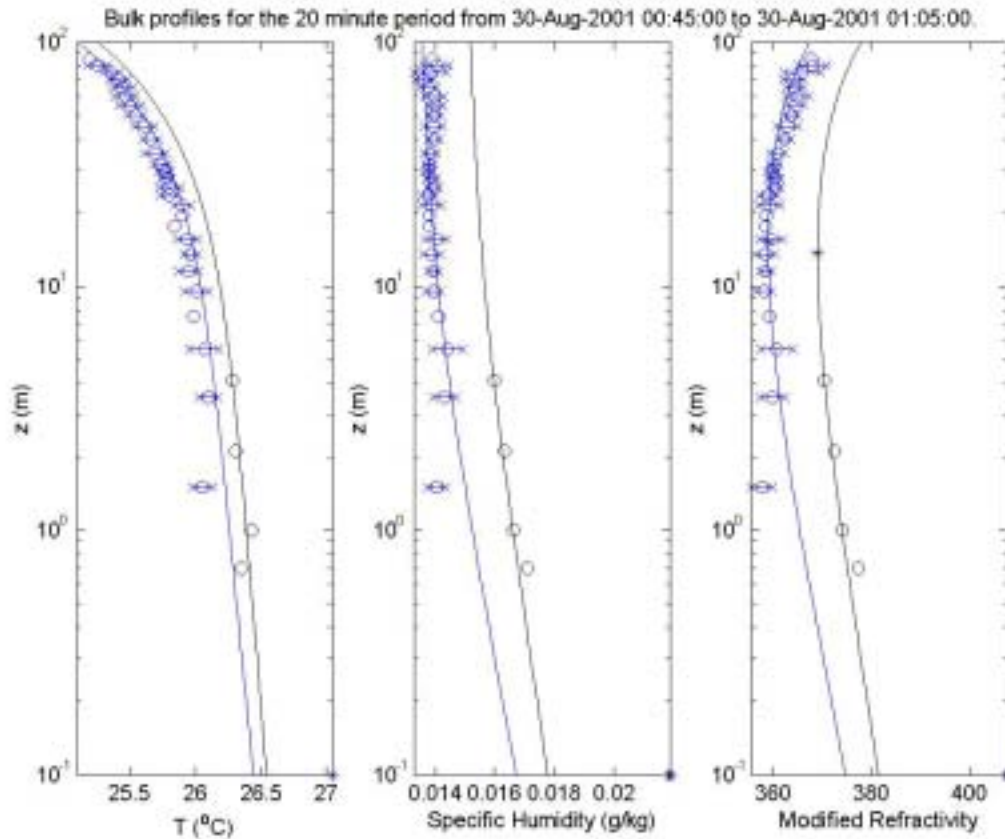


Figure 11. Profiles of temperature, specific humidity and modified refractivity versus height (log scale). Black circles are buoy data. Blue circles are kite-borne radiosonde data. Bars associated with blue circles represent plus and minus one standard deviation. Blue circles without associated bars are averages of less than ten data points. Solid lines are bulk profiles. The black solid line is computed from the 4.08-meter buoy data. The blue solid line is computed from the 19.5-meter kite-borne radiosonde data.

In general, the kite refractivity values were approximately ten M-units too small when compared with the buoy values (see Fig 11 above). It has recently been shown that the RS-80 humidity sensor can develop a dry bias while stored for as little as three to four months (Henson, 2002). Therefore, we assumed that the radiosonde humidity was too low and the buoy was correct.

Since it is the gradient of M and not M itself that is important in determining propagation, the kite values were adjusted to match up with the buoy values. The calibration procedure involved fitting both the kite data only and the buoy data only with quadratic functions (Fig 12, left panel). The mean difference between the two

polynomials for the region between the top buoy value and the bottom kite value was used to adjust all kite values (Fig 12, right panel).

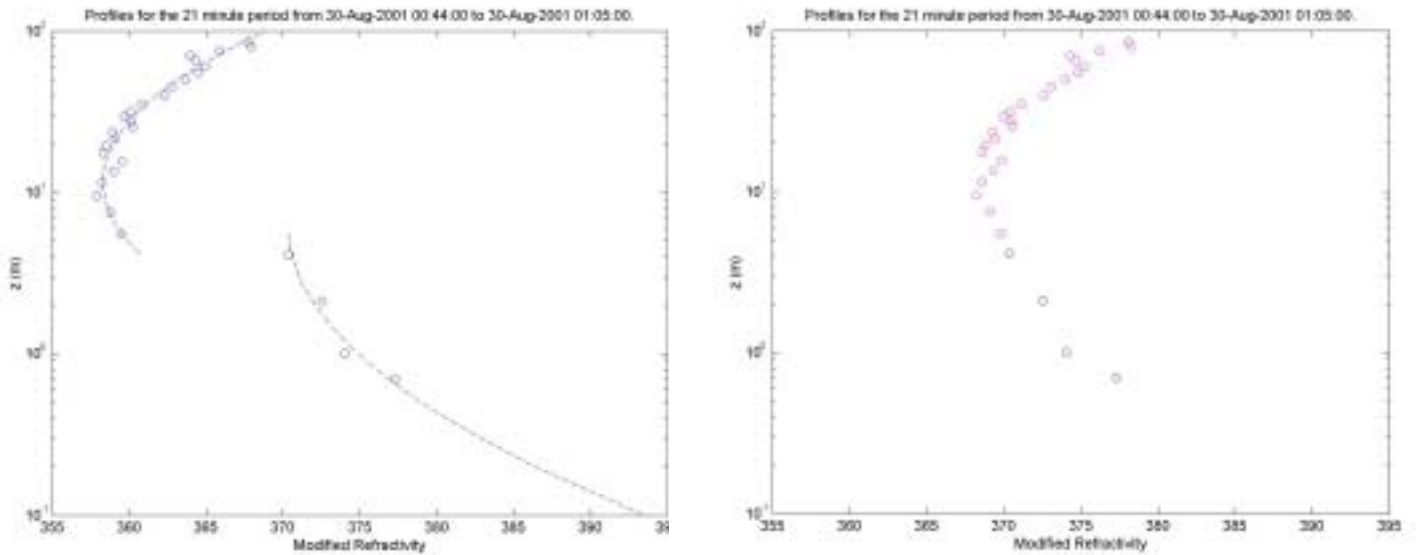


Figure 12. Left panel shows actual kite-borne radiosonde data (blue circles) and buoy data (black circles) with quadratic functions fit to them. Right panel shows the same buoy data with the adjusted kite-borne radiosonde data (magenta circles).

The buoy data (including the surface value based on the infrared sea surface temperature) combined with the kite data from 5.5 m to 100 m were fit to the natural logarithm of height with a quartic function. Adding 0.1 m to each height before the fit was done and subtracting the same amount afterward overcame the problem of finding a value of M for the surface.

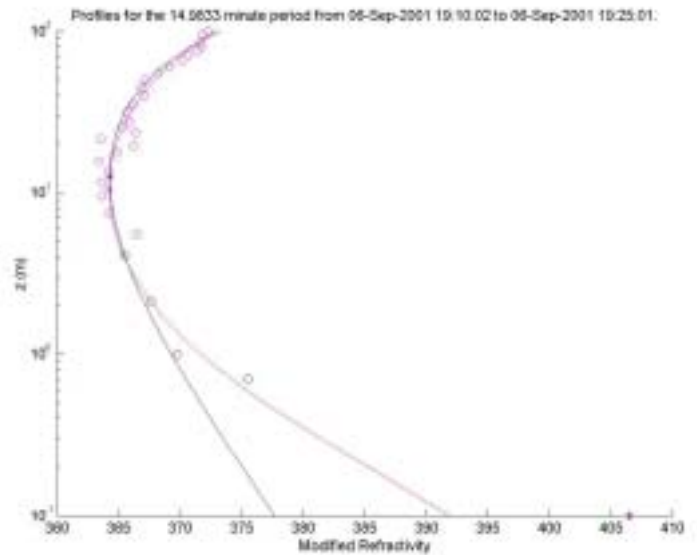
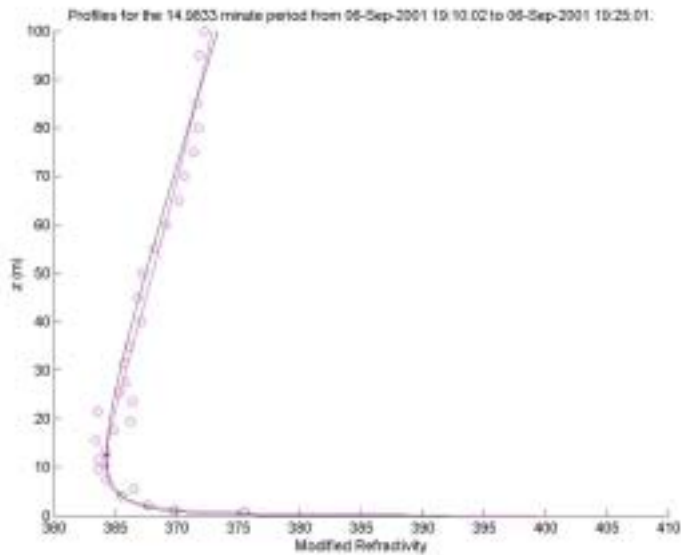


Figure 13. An example (linear height scale on the right, log on the left) of a case when the bulk profile from the buoy data (black line, procedure described below) and the smoothed profile from the kite-borne radiosonde data merged with the buoy data (magenta line, procedure described above) match extremely well above 3.5 m.

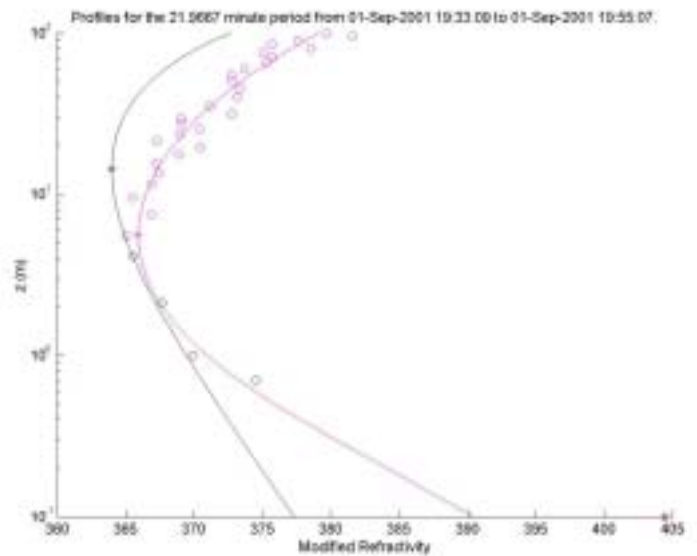
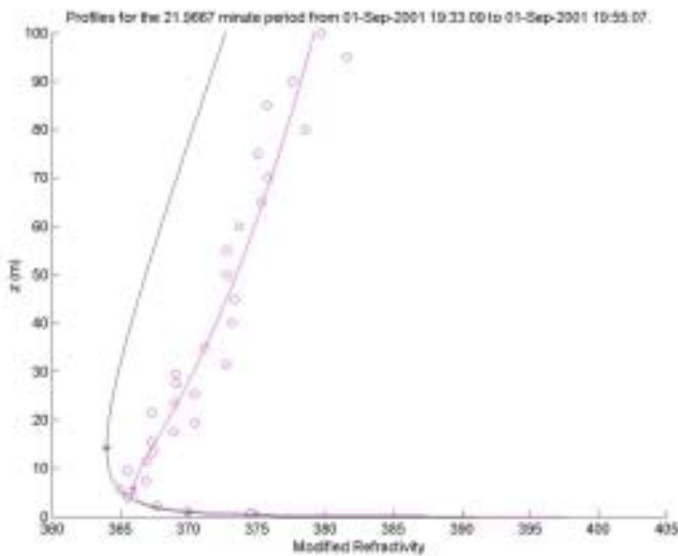


Figure 14. An example (linear height scale on the right, log on the left) of a case when the bulk profile from the buoy data (black line, procedure described below) and the smoothed profile from the kite-borne radiosonde data merged with the buoy data (magenta line, procedure described above) match poorly at all levels. Cases like this are rare.

The buoy profile data alone could not be used to create a reasonable smoothed profile of M up to the evaporation duct height. Since the evaporation duct height (the height of the minimum value of M) generally occurred above four m, any polynomial fit to the four buoy data points would be monotonically decreasing with height, which is unrealistic.

2. Bulk Method Results

The generated bulk profiles from the buoy data used the same averaging periods as the smoothed results. The temperature and relative humidity values from 4.08 m, in addition to the pressure and wind speed data, were used with the bulk model described above. Examples of the results can be seen in Figs 11, 13 and 14 (black lines).

3. Summary of Environmental Profiles

When comparing the bulk and smoothed profiles, it is important to note that the slope of the modified refractivity profiles, not the values themselves, are important in determining propagation. In general, the two types of profile are in good agreement above 3.5 m; the differences in both value and gradient are well within one standard deviation of zero. Below 3.5 m, except in the lowest ten cm, the smoothed profiles exhibit stronger negative gradients than the bulk profiles (differences noted peaked at 38 m^{-1}). Conversely, the bulk profile has an extremely strong negative gradient in the lowest ten cm (the mean difference was 125 m^{-1}).

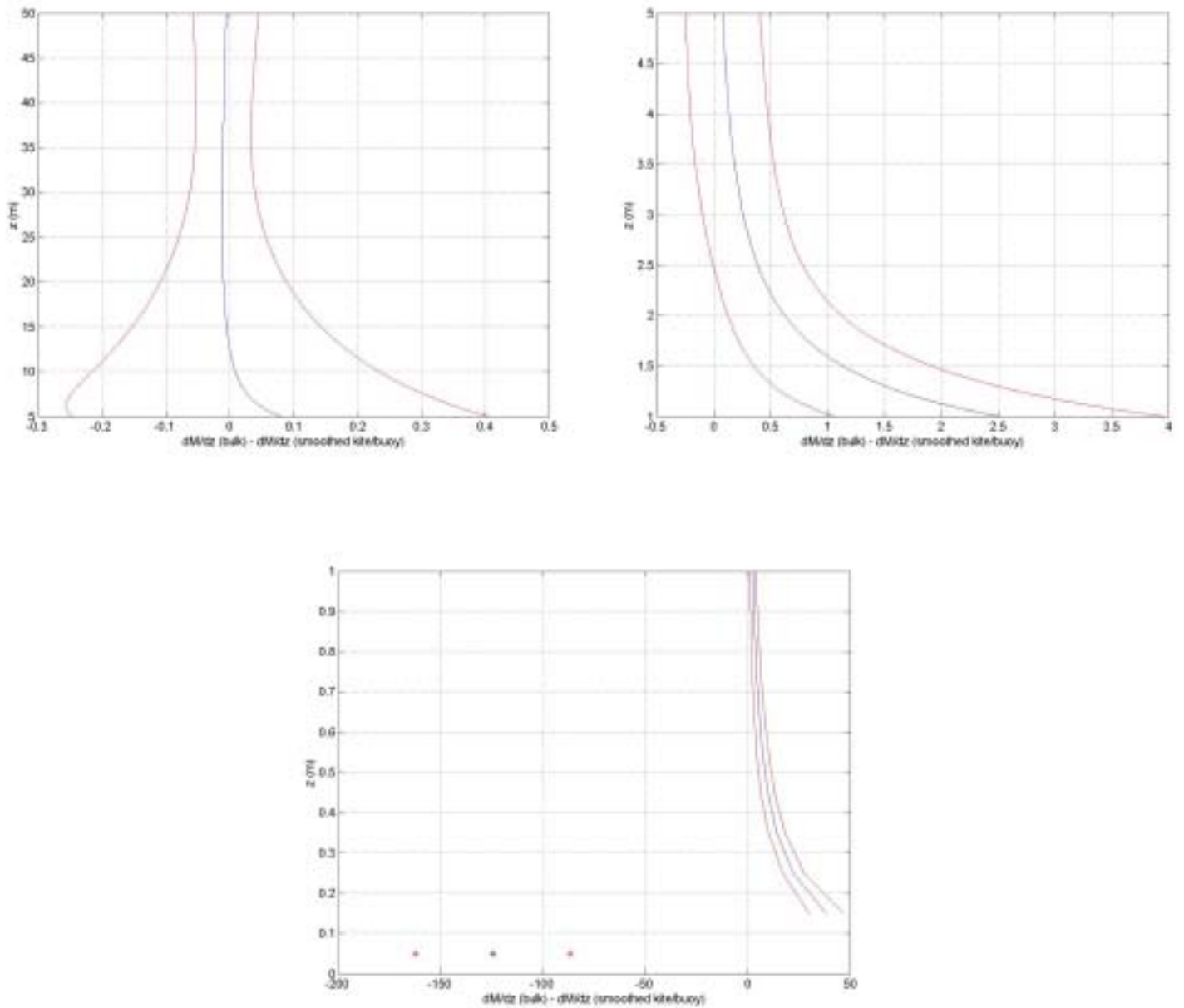


Figure 15. Blue lines represent the mean difference between the first order approximations of dM/dz (45 averaging periods). Red lines represent plus and minus two standard deviations. Top left panel is from five to 50 m. Top right panel is from one to five m. Bottom panel is from the surface to one m. Asterisks are used for the 0.05-meter values.

	$M_{\text{bulk}} - M_{\text{smoothed}}$		$dM/dz_{\text{bulk}} - dM/dz_{\text{smoothed}}$	
	Mean	Std	Mean	Std
$z < 0.1 \text{ m}$	-0.0317	0.0508	-125	18.9
$0.1 \text{ m} \leq z < 1 \text{ m}$	-5.24	1.28	11.9	1.76
$1 \text{ m} \leq z < 3.5 \text{ m}$	-0.548	0.423	0.711	0.284
$3.5 \text{ m} \leq z < 5 \text{ m}$	0.110	0.444	0.122	0.168
$5 \text{ m} \leq z < 12.4 \text{ m}$	0.320	1.02	0.0230	0.126
$12.4 \text{ m} \leq z < 50 \text{ m}$	0.194	2.11	-0.00924	0.0355

Table 3. Mean and standard deviation of the difference between the values and gradients of modified refractivity of bulk and smoothed profiles based on 45 averaging periods. The information in the two right-hand columns is the same as that presented in Fig 15.

THIS PAGE INTENTIONALLY LEFT BLANK

IV. PROPAGATION PREDICTIONS

A. AREPS CONFIGURATION

The planners of the RED experiment designed it to evaluate and formulate RF/EO propagation models. Using the U. S. Navy's operational RF propagation model, AREPS, this study tested each of the six frequency/antenna height configurations against three refractivity profiles for each averaging period. The refractivity profiles used to generate environments in AREPS were: 1) the bulk predictions based on mean data at a single airflow level, as well as sea surface temperature, from the buoy, 2) the regression fit to the merged kite-borne radiosonde and buoy-measured profile data, and 3) the standard atmosphere available in AREPS.

AREPS (research mode) calculated propagation loss using the above environmental inputs as well as the parameters shown in Table 4.

Frequency (MHz)	2975, 9700, 17700
Vertical Beam Width (degrees)	20
Elevation Angle (degrees)	0
Polarization	Horizontal
Antenna Type	Gaussian
Antenna Height (m)	4.88, 12.62 (nominal, adjusted based on actual height data from R/V FLIP)
Receiver Height (m)	4.73 (nominal, adjusted based on changes in mean sea level)

Table 4. AREPS parameters.

The procedure was to compute propagation loss versus distance for each combination of averaging period, profile, frequency and antenna height, i.e. 45 averaging periods, three types of profiles, three frequencies and two antenna heights. The antenna and receiver heights chosen were based on the mean antenna and receiver heights for the closest five-minute time period when propagation loss measurements were available.

This resulted in a total of 810 separate model-generated solutions for propagation loss versus distance. The measure of the atmospheric effects presented in most of the following interpretations is propagation factor, which was obtained by subtracting the appropriate free space propagation loss, also generated by AREPS, from either model-generated or measured propagation loss.

B. WARM-WATER RESULTS

Since the primary purpose of this study is to compare bulk profiles of modified refractivity to directly measured profiles of modified refractivity, this thesis presents several examples of the predicted effects of these differences on propagation. The first three effects comparisons considered (Figs 16, 17, and 18) are for the S-, X- and Ku-Band predictions, respectively, for the environments shown in Fig 14. This was a case when the shape of the smoothed profile based on the merged buoy and kite data was very different from the bulk profile at every level. The next three effects comparisons considered (Figs 19, 20, and 21) are also for the S-, X- and Ku-Band predictions, respectively, but for the environments shown in Fig 13. This was a case when the shape of the smoothed and bulk profiles were almost identical, except in the lowest 3.5 m.

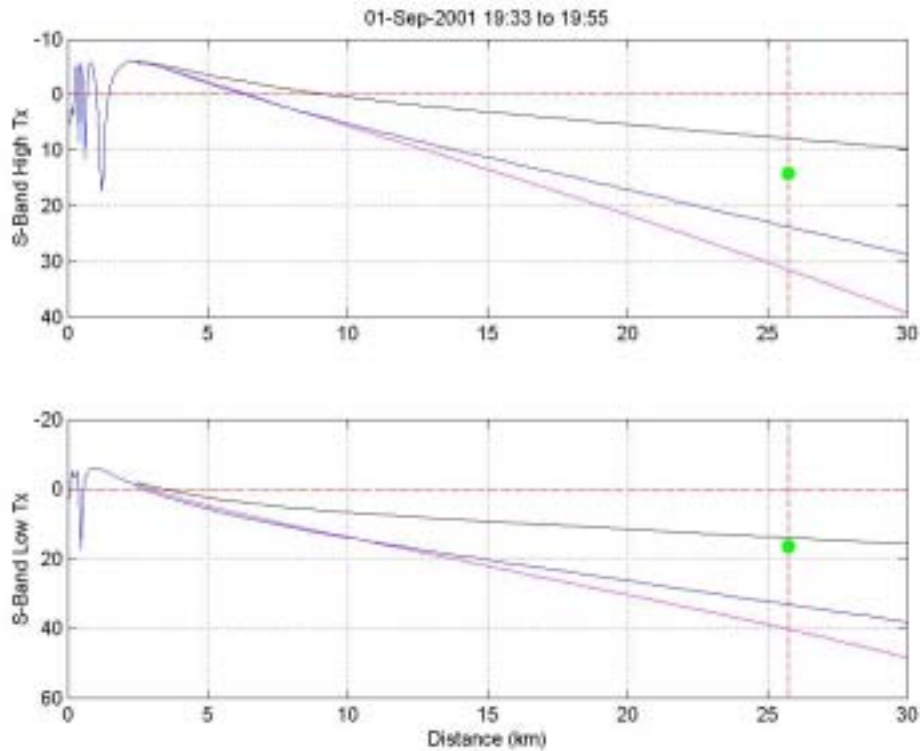


Figure 16. S-Band propagation factor versus distance for September 1, 2001 from 1933 to 1955 UTC. The vertical axis of each plot is propagation factor (propagation loss predicted minus propagation loss in free space, measured in dB). The horizontal red dashed line represents a propagation factor of zero; propagation loss equal to free space propagation loss. The horizontal axis of each plot is distance measured in km. The vertical red dashed line represents the length of the propagation path during the RED experiment. The black line represents propagation factor based on the bulk profile of modified refractivity. The magenta line represents propagation factor based on the smoothed profile from the merged buoy and kite data. The blue line represents propagation factor based on the standard atmosphere. The green dots represent measured values of propagation loss for the appropriate frequency, antenna height, and time period (converted to propagation factor by subtracting the appropriate propagation loss in free space). The top panel is for the higher antenna and the bottom panel is for the lower antenna.

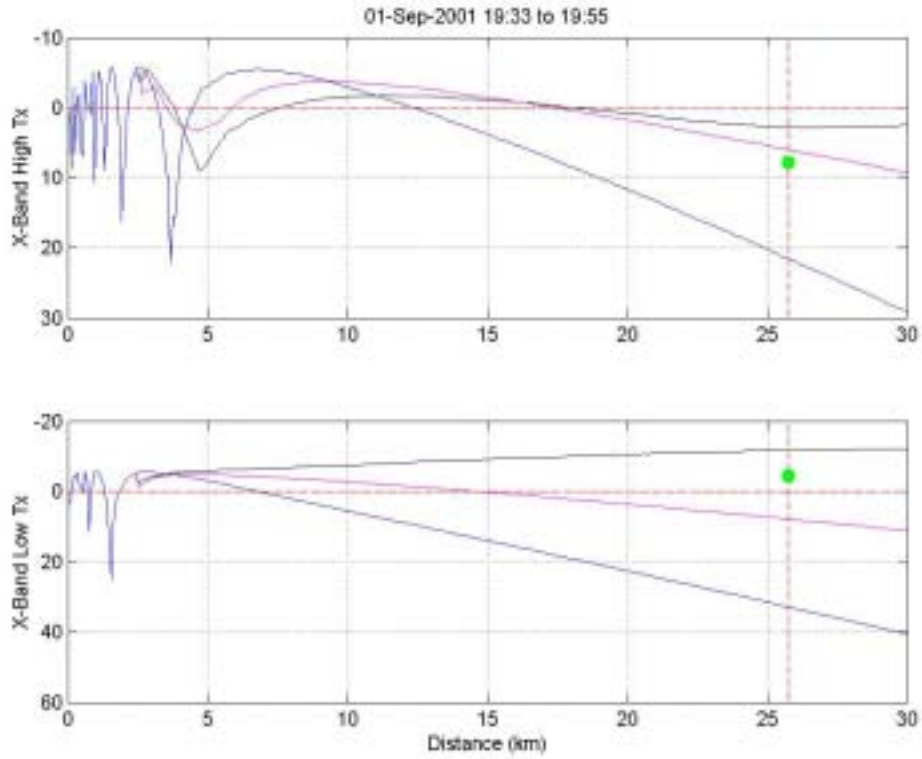


Figure 17. As above, but for X-Band.

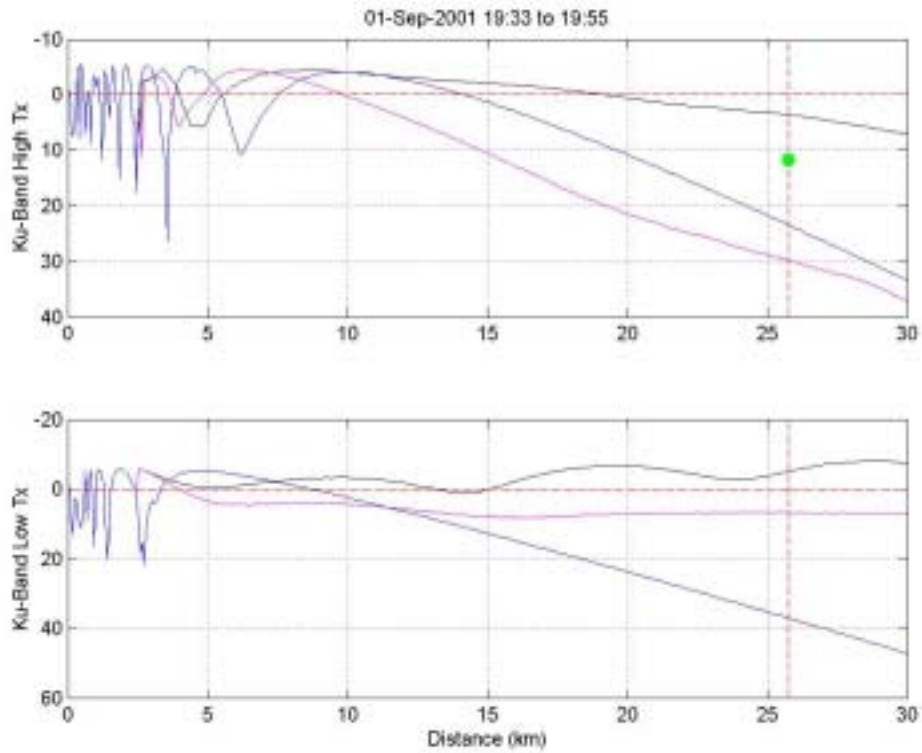


Figure 18. As above, but for Ku-Band.

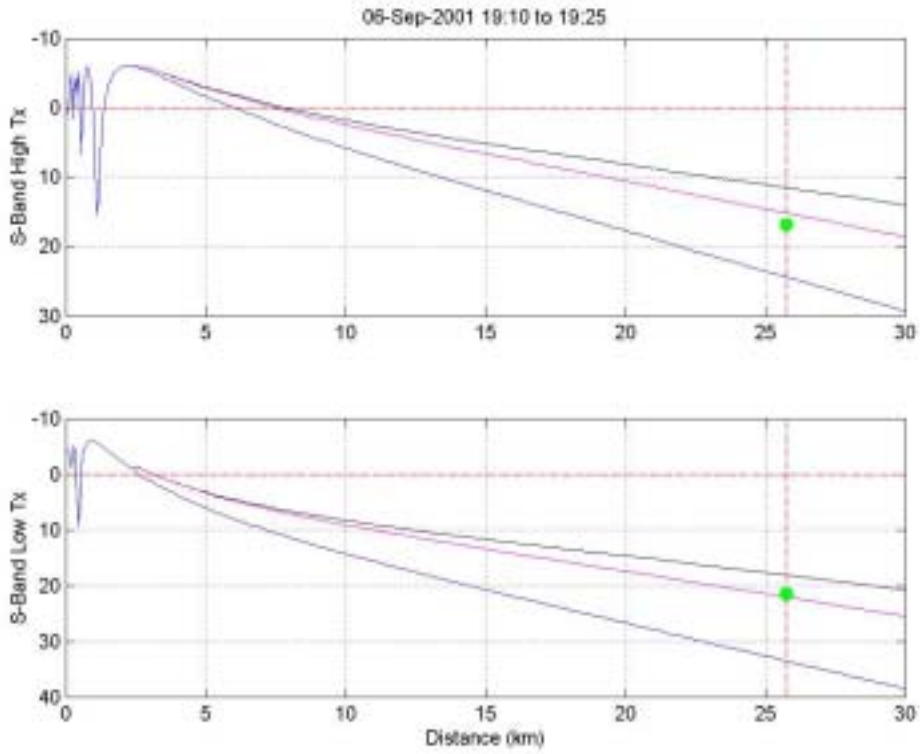


Figure 19. As in figure 16, but for September 6, 2001 from 1910 to 1925.

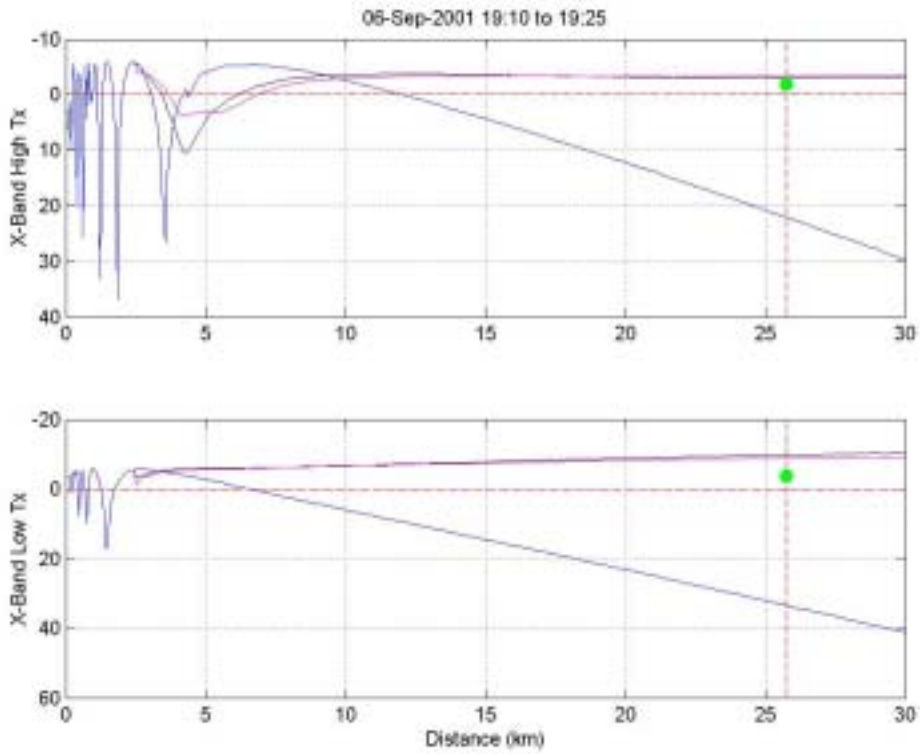


Figure 20. As above, but for X-Band.

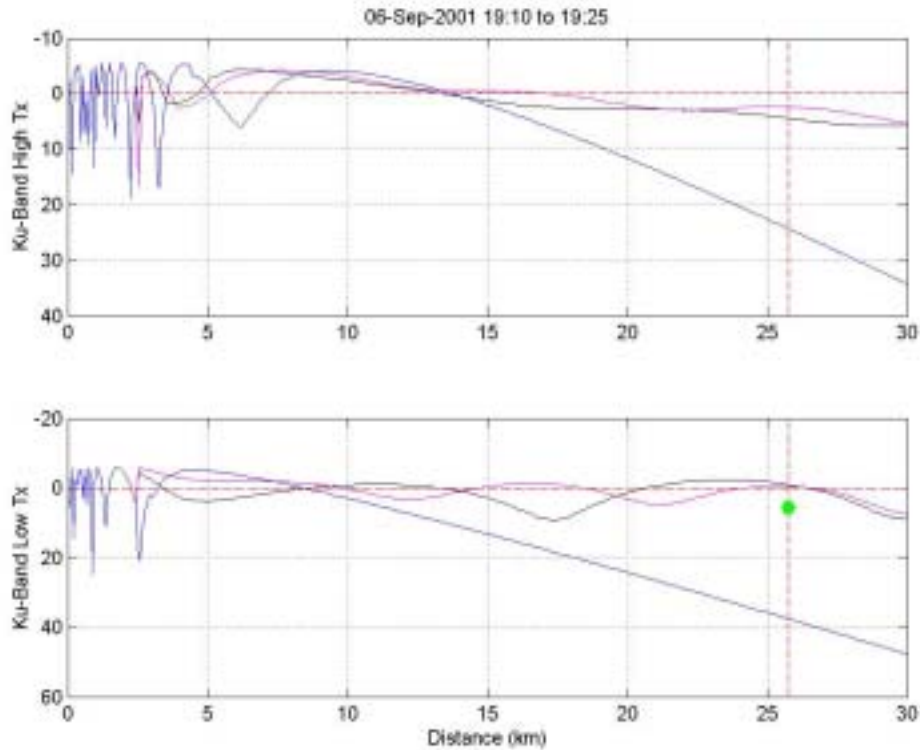


Figure 21. As above, but for Ku-Band.

Fig 19 shows the most interesting comparison. This is associated with the environmental case in which the merged and bulk profiles used to generate these propagation predictions were almost identical above 3.5 m. It follows that the increased propagation loss predicted from the smoothed profile in the S-Band is most likely due to the steeper gradient of M from 3.5 m down to 10 cm (and/or the much less steep gradient from 10 cm to the surface).

As stated previously, the above six figures represent only two out of 45 averaging periods available. Since it is not feasible to show all the results as propagation factor versus distance, this thesis presents the results as a summary. Figs 22 through 27 summarize the comparison of predicted propagation loss values at 25.77 km with the measured loss values for the appropriate frequency, antenna height and averaging period.

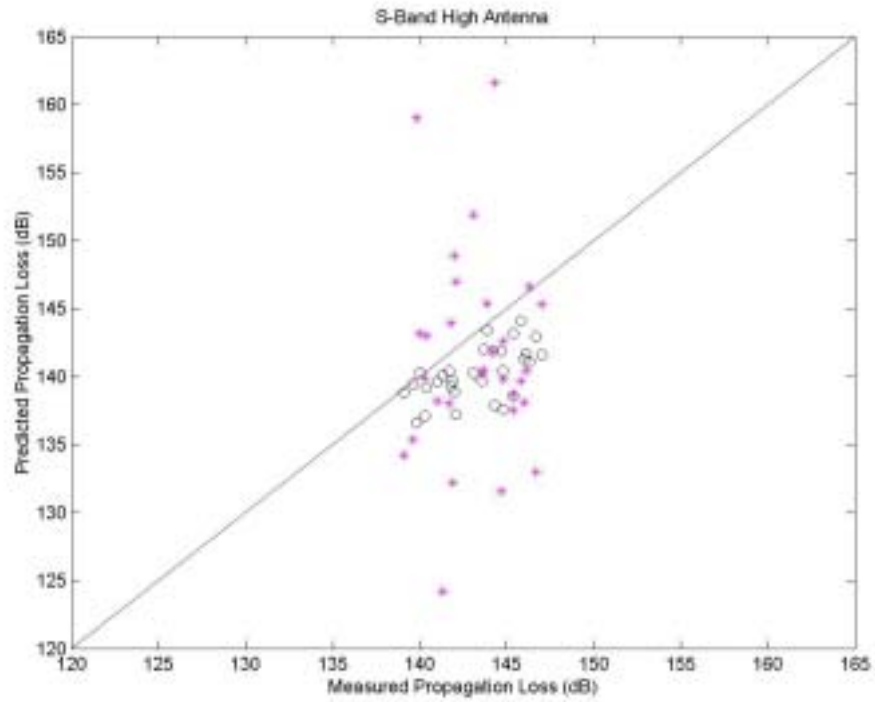


Figure 22. Summary of predicted versus measured propagation loss for the high antenna S-Band. Black circles represent predictions from bulk profiles. Magenta asterisks represent predictions from smoothed profiles of merged kite and buoy data.

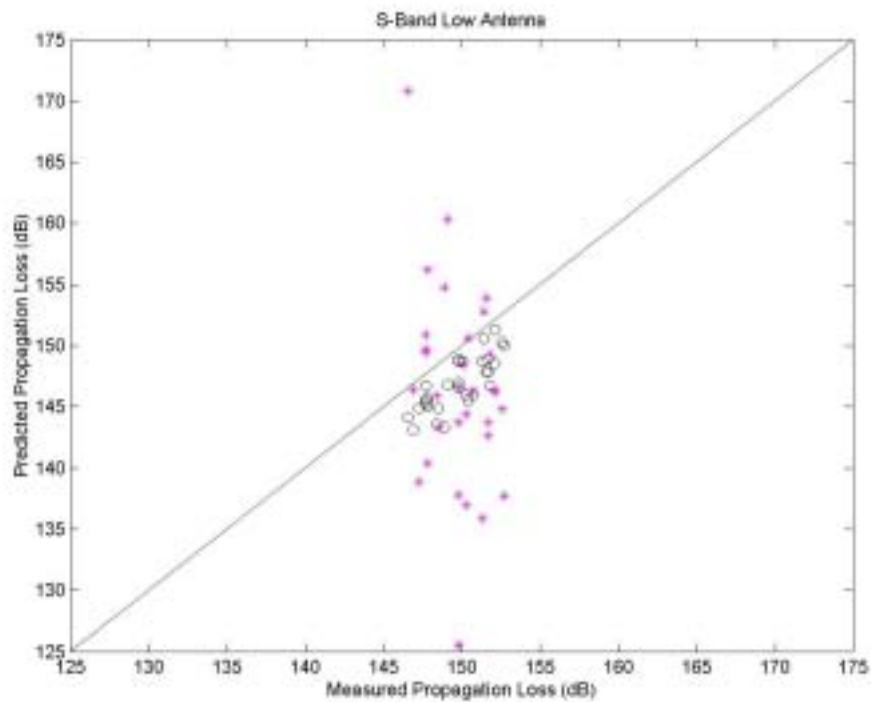


Figure 23. As above, but for the low antenna S-Band.

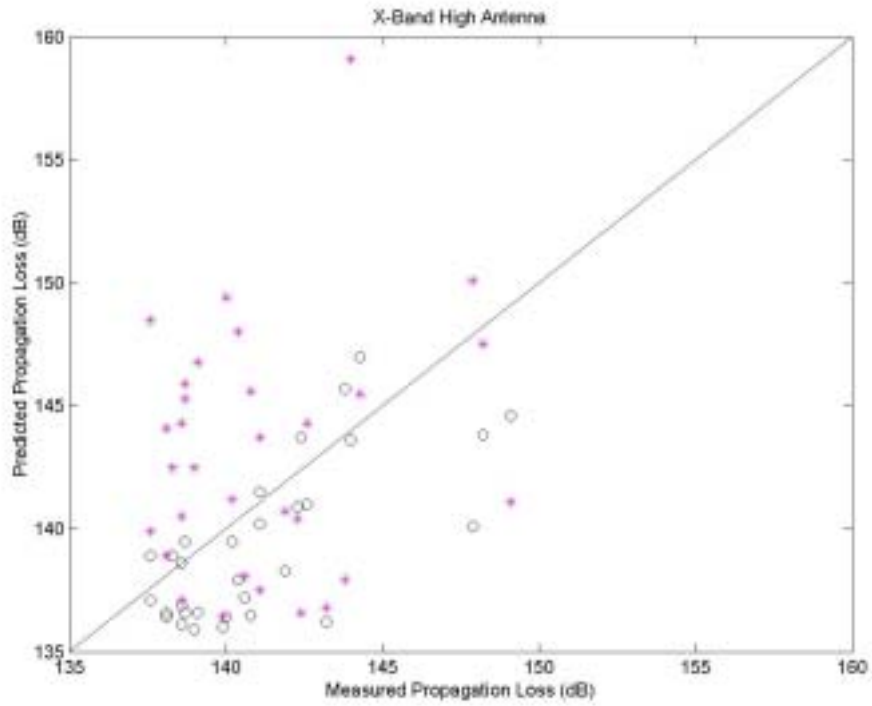


Figure 24. As above, but for the high antenna X-Band.

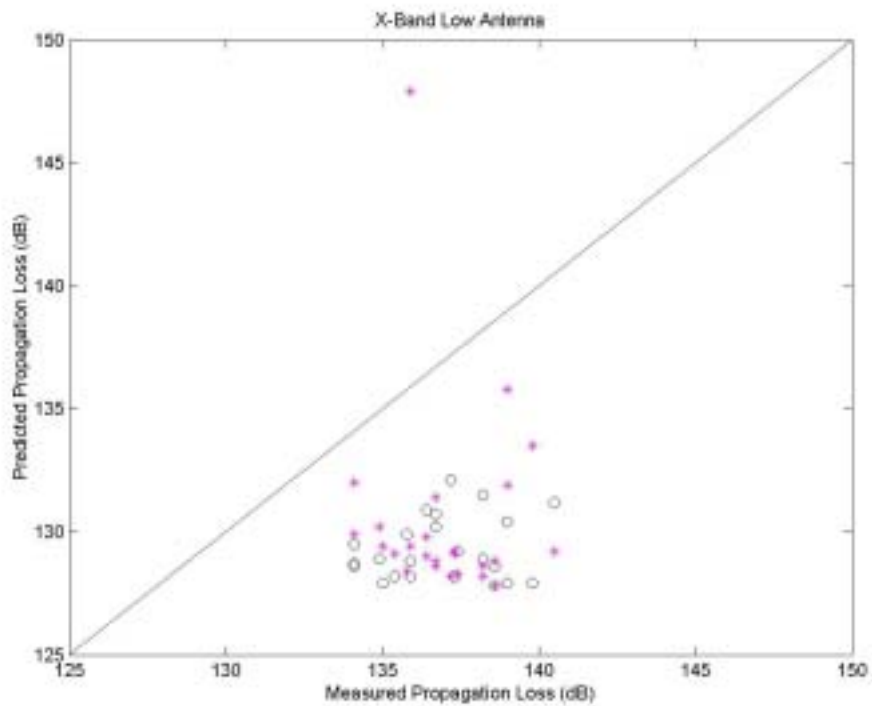


Figure 25. As above, but for the low antenna X-Band.

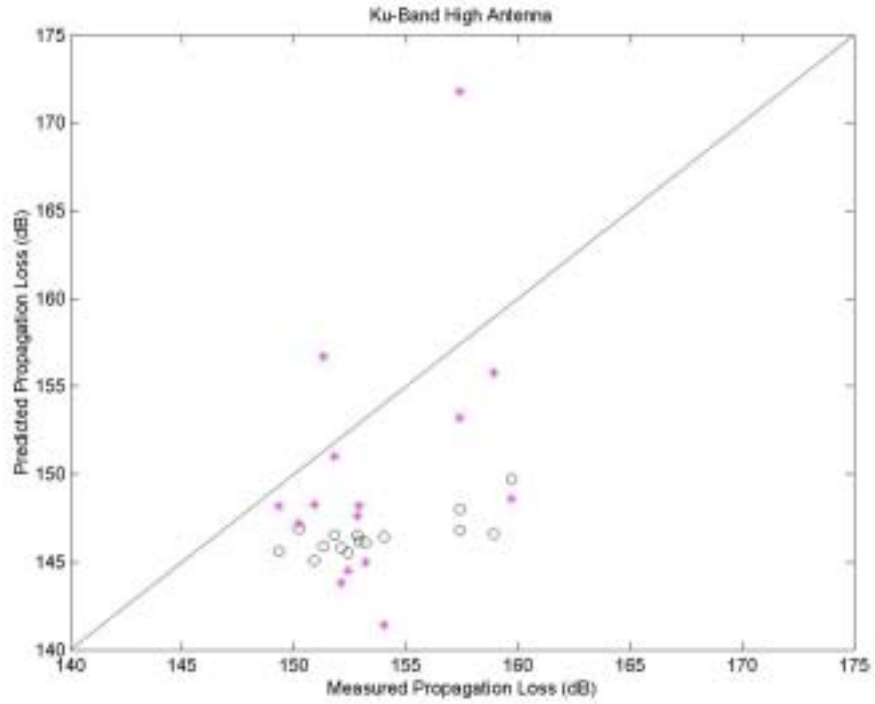


Figure 26. As above, but for the high antenna Ku-Band.

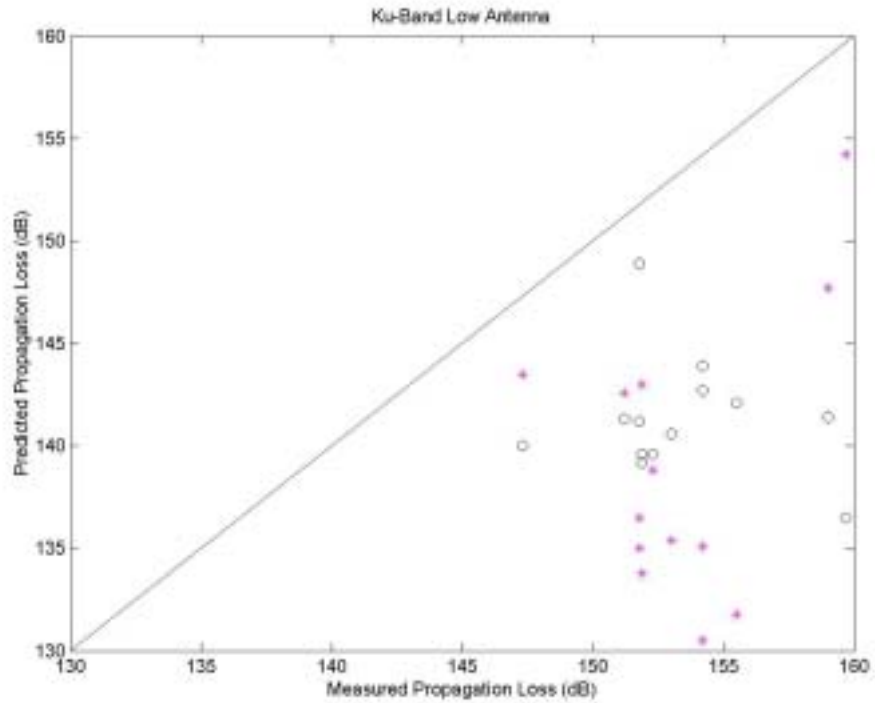


Figure 27. As above, but for the low antenna Ku-Band.

Comparison results in Figs 22 through 27 show that propagation predictions based on the smoothed profiles generated from merged kite-borne radiosonde and buoy data are much more variable than either the propagation measurements or the propagation predictions based on bulk profiles. Table 5 summarizes these variability differences and also the predictive quality of the two types of profile (shown as correlation coefficient with the measured propagation).

	Propagation Measurements During Kite Operations	Standard Deviation			Correlation with Propagation Measurements	
		Measured Propagation	Bulk	Merged	Bulk	Merged
S-Band High Antenna	31	2.3432	2.0564	7.1548	0.5788	0.0090
S-Band Low Antenna	32	1.8081	2.4373	8.6209	0.7912	-0.2696
X-Band High Antenna	32	3.0678	3.0416	4.7987	0.6981	0.1874
X-Band Low Antenna	26	1.7575	2.0661	4.6994	0.1304	-0.0349
Ku-Band High Antenna	15	3.2203	3.4926	6.3617	0.7341	0.4205
Ku-Band Low Antenna	14	3.5515	2.7338	7.6837	-0.1044	0.2376

Table 5. Comparison of variability and predictive capability of bulk and merged profiles of modified refractivity.

For the S-Band, the bulk profiles produced consistently low predictions of propagation loss, but were able to capture some of the variability of the measurements. The merged profiles showed no skill in predicting propagation loss. For the X-Band, the bulk profiles again showed some forecast skill, but only for the high antenna. Both types of profiles had poor propagation loss predictions for the low antenna in the X-Band. For the Ku-Band, the bulk profile propagation loss predictions did show a modest increase as actual propagation loss rose, but the skill of these predictions is not as great as the high correlation coefficient in Table 5 seems to indicate. With the exception of two outliers, Fig 26 shows that the merged profiles provide relatively better predictions of propagation loss compared to the bulk profile predictions, but they were still poor. For the low antenna in the Ku-Band, as in the X-Band, neither profile was useful in predicting propagation loss.

C. COLD WATER RESULTS

As noted previously, contamination of the temperature and relative humidity records was a problem during the cold-water experiment due to the larger ship size. Even when the contaminated data was removed, the bottom two bins (1.5 and 3.5 m) proved

unreliable, just as they were during RED. For this set, there was no alternative source of near-surface profile data that could be merged with the kite data to create smoothed profiles. Therefore scientific objectives in comparing profile shapes and propagation predictions for profiles of modified refractivity generated from bulk methods and direct measurements could not be met in a similar manner for the cold-water experiment as they were for RED, the warm water experiment. Objectives to compare propagation as predicted by in situ derived profiles with observed propagation are still possible. However, they are outside the scope of this unclassified thesis.

THIS PAGE INTENTIONALLY LEFT BLANK

V. SUMMARY

A. PRESENT STUDY LIMITATIONS

Unexpectedly, the directly measured profiles led to much greater variability in propagation predictions than the bulk profiles (despite the similarities in the profiles themselves above 5 m, see Fig 15). Reasons for this are not clear. After final editing and analyses are performed on the propagation data and extended analyses and editing of the complete atmosphere and ocean surface data set, including other platforms and wave information, are completed, the reasons for the poor results may become more obvious. It is concluded that the manner in which the data were collected and analyzed leaves several questions to be answered, many worthy of future studies with these data sets and also through the design and implementation of future field collections.

1. Kite-borne radiosonde

The kite-enabled direct collection of modified refractivity profiles along the propagation path from just above the surface to above 100 m, although extremely important to the overall experimental goals, proved to be very challenging. Although the use of a kite to collect data a significant distance from the ship is viable, several resolution and accuracy issues surfaced.

a. Vaisala RS-80 radiosonde

Many of the kite-borne radiosonde data analysis problems could possibly have arisen from the use of this particular model of radiosonde. The RS-80 is designed to be rugged and economical (Vaisala, 1998) for operational measurement of profiles to the top of the troposphere. It was not designed for the precision, accuracy and fast response time required to create high-resolution profiles of modified refractivity all the way down to the surface. Using a more accurate, precise and faster responding but also more expensive and delicate, instrument to record pressure, temperature and humidity would resolve the following issues. The suggestions offered below, therefore, are limited to the assumption that the RS-80 is the only instrument available.

1) Height

The method of height correction certainly introduced errors. The lack of height accuracy and resolution, combined with the fact that the height above the actual air/water interface changed (even as measured pressure remained constant) as the radiosonde moved over crests and troughs, probably contributed to the poor quality of the lowest two bins of data (1.5 m and 3.5 m) collected from the kite-borne radiosondes. A low cost solution to this problem would be the suspension of some highly visible, rigid, extremely lightweight material of fixed length (approximately one to two m) to the bottom of the radiosonde. If the times when this material entered the water were recorded precisely, the pressure record could be adjusted accordingly. This would take advantage of the one-meter resolution of the RS-80.

2) Humidity

Based on a study of over 8000 radiosonde launches during TOGA-COARE, an algorithm has been developed to correct the dry-bias noted during that experiment. Upon publication, this algorithm could be adapted and applied to the kite-borne radiosonde data collected during RED. Alternatively, as suggested by Junhong Wang of the Atmospheric Technology Division of the National Center for Atmospheric Research, a ground-truth comparison could be done prior to collecting data with the kite-borne radiosonde. For an experiment with a design similar to that used in RED, this could be accomplished by flying each radiosonde in the vicinity of a buoy with more accurate humidity sensors than the radiosonde itself.

b. Data Matching

If the humidity measurement issue described above were addressed, the problem of matching the kite-borne radiosonde data with the buoy data would likely be minimized. The problem, however, is still an important one to address. For example, radiosondes launched from ships do not collect enough near-surface data for evaporation ducts to be resolved (Baldauf, 1997) and matching radiosonde data to bulk profiles may provide the best solution.

Quadratic functions were used to merge the kite and buoy data sets because matching the averaged values at any particular height yielded unrealistic profiles. An alternative method would be to adjust the kite-borne radiosonde data to minimize the error with a bulk profile generated from one of the buoy levels. This would obviously, however, undermine one of the main purposes of this study, which was to compare the bulk profile with the directly measured profile.

2. Averaging Period Selection

As mentioned previously, the averaging period selection was entirely subjective. A more rigorous approach would apply specific criteria: time period upper and lower limits, and upper limits on the variability of wind speed, wind direction, temperature, humidity and sea surface temperature. This would make averaging period selection an automatic process and would also allow the effects of varying the selection criteria to be investigated.

3. Profile Smoothing

The choice of the quartic polynomial to smooth the merged kite and buoy data was based on subjective inspection of polynomials up to order six. More complicated functions were not considered. This led to a good match between the merged data profiles and the bulk profiles above 3.5 m, as seen in Fig 15. The difference in gradient below 3.5 m seems real (and not just a result of the smoothing), especially based on the buoy measurements at 0.71 m.

4. Propagation Prediction and Measurement

Even assuming the kite-borne radiosonde measurements, the method by which they were matched to the buoy data and the manner in which these merged data sets were smoothed provide an accurate description of the profile of modified refractivity, a comparison of predicted and measured propagation loss still may not yield conclusive results.

a. Measured Propagation Loss

In order to draw any conclusions from such a comparison, the measurements of propagation loss must be extremely reliable and also available during the specific times when the kite-borne radiosondes were operated. Unfortunately, several

of the kite-borne radiosonde operations occurred during times when propagation measurements were either not available or undergoing extreme transients (Fig 28).

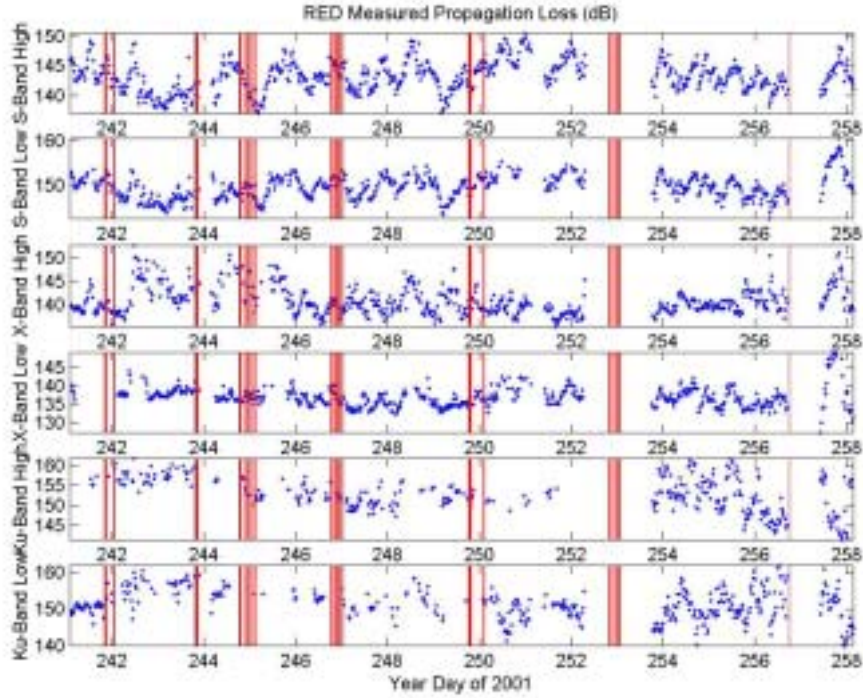


Figure 28. Time series showing propagation measurement availability (blue dots) and kite-borne radiosonde averaging periods (red vertical lines).

b. Variability of Refractivity Conditions Along the Propagation Path

The AREPS propagation predictions used a single profile to represent the entire 25.77 km path. This favored the bulk profiles because the bulk method is based on average conditions while the smoothed profiles only reveal the conditions at a specific location. Future work with the data collected during RED should include propagation predictions using multiple smoothed profiles to represent refractivity conditions along the propagation path.

B. CONCLUSIONS

1. Profiles of Modified Refractivity

The gradients of modified refractivity determined using bulk methods and obtained from direct measurement (using data from kite-borne radiosonde merged with buoy data) showed good agreement above 3.5 m (see Fig 15 and Table 3). Between 3.5

m and ten cm, buoy-based profile data indicates that the humidity gradient is stronger than predicted by bulk methods (leading to a stronger gradient of modified refractivity). Reasons for this disagreement should be the subject of future work with the data obtained during RED as well as motivation for the design of future experiments.

2. Propagation Predictions

Propagation predictions based on smoothed profiles of direct measurements of modified refractivity show much more variability than predictions based on profiles generated using bulk methods for all frequencies. Propagation predictions based on smoothed profiles of direct measurements of modified refractivity show little correlation with measured propagation at any frequency. In the S-Band (and for the X-Band transmitted from the higher antenna), propagation predictions based on bulk profiles show good correlation with measured propagation. This phenomenon could be further investigated by using AREPS to generate propagation predictions for environmental profiles that slowly varied from a bulk shape to a merged shape.

THIS PAGE INTENTIONALLY LEFT BLANK

LIST OF REFERENCES

- Baldauf, B. K., 1997; Evaluation of Low Altitude Rocket Dropsondes (Rocketsonde) for EM Propagation Assessment. *Navy EM/EO Symposium 2-6 Jun 1997, Monterey, CA*, 421-429.
- Davidson, K. L., 2002; Assessment of Atmospheric Factors in EM/EO Propagation, *Class Notes for MR4416, Naval Postgraduate School, Monterey, CA*.
- Fairall, C. W., E. F. Bradley, D. P. Rogers, J. B. Edson, and G. S. Young, 1996; Bulk Parameterization of Air-Sea Fluxes for Tropical Ocean-Global Atmosphere Coupled-Ocean Atmosphere Response Experiment. *Journal of Geophysical Research*, **101**, No. C2, 3747-3764.
- Henson, R., 2002; How Dry They Are: Public-Private Team Fixes Sounding Bias. *UCAR Quarterly*, Spring 2002, 6.
- Kimbrell, T. W., 2001; Evolution of Naval Radar Technology--A Convergence of Requirements and Technology. *Personal Communication*.
- O'Connor, A., 2001; Physics of Atmospheric Refraction and AREPS Demonstration, http://www.nmopdc.navy.mil/PPT/EM_Propagation.pdf.
- Sanabia, E. R., and R. C. Easton, 2000; Exploiting the Environment to Win in the 21st Century, White Paper of 14 Dec 00. USS Port Royal (CG 73), Fleet Post Office, AP 96675-1193, 3140 Ser 00/0207.
- Vaisala, 1998; Technical Information--RS80 Radiosonde, http://www.vaisala.com/DynaGen_Attachments/Att2745/2745.pdf.

THIS PAGE INTENTIONALLY LEFT BLANK

INITIAL DISTRIBUTION LIST

1. Defense Technical Information Center
8725 John J. Kingman Road, Suite 094
Ft. Belvoir, VA 22060-6218
2. Dudley Knox Library
Naval Postgraduate School
411 Dyer Road
Monterey, CA 93943-5101
3. The Oceanographer of the Navy
United States Naval Observatory
3450 Massachusetts Avenue, NW
Building 1
Washington, DC 20932-5421
4. Dr. R. Ferek, Code 322 MM
Office of Naval Research
800 North Quincy Street
Arlington, VA 22217-5660
5. Professor Kenneth L. Davidson, MR/DS
Department of Meteorology
Naval Postgraduate School
589 Dyer Road, 254 Root Hall
Monterey, CA 93943-5114
6. Dr. Robert E. Gover, Code 5753.00
Naval Research Laboratory 3310
Washington, DC 20375-5328
7. G. Daniel Dockery
The Johns Hopkins University/Applied Physics Laboratory
Johns Hopkins Road
Laurel, MD 20720-6099
8. Richard Paulus
SPAWARSYSCEN-SD, 2858
53560 Hull Street
San Diego, CA 92152
9. J. Stapleton, Code T44
Naval Surface Warfare Center, Dahlgren Division (NSWCDD)
Dahlgren, VA 22448

10. Commander
Space and Naval Warfare Systems Command (PMW-155)
4301 Pacific Highway
San Diego, CA 92110-3127

11. Thomas Piwowar
Space and Naval Warfare Systems Command
4301 Pacific Highway
San Diego, CA 92110-3127

12. Kenneth Anderson
SPAWARSYSCEN-SD, 2858
53560 Hull Street
San Diego, CA 92152

13. Frank Ryan
SPAWARSYSCEN-SD
53560 Hull Street
San Diego, CA 92152